AN ABSTRACT OF THE THESIS OF

David C. Irving for the degree of Master of Science in Forest Products presented on January 16, 1989.

Title: A Study of Load-induced Microdeformations within Wood-based Structural Members using Optical Scanning Techniques

Signature redacted for privacy.

Abstract approved: ~~Dr. Phillip~~ E. Humphrey

Efficient use of wood in structural applications depends upon the accuracy with which we can predict the mechanical behavior of members under load. Most methods of lumber grading and laminated beam design depend upon statistical and/or empirical techniques in which averaged properties for complete members are derived. A knowledge of stresses and strains that develop locally within members as they are loaded would provide a more complete picture of the interactions that combine to affect the behavior of complete members. Wood's anisotropic, porous, and hygroscopic nature has limited the use of many conventional methods to experimentally obtain this information. This paper describes a technique for studying microdeformations within wood-based specimens under flexural loading in which computerised optical scanning (machine vision) is used.

Specially prepared beams containing laminae of varying elastic moduli and defects were loaded nondestructively in third-point flexure while being supported laterally to prevent buckling. Beam width was reduced to 0.25" to avoid significant gradients of strain perpendicular to the measured surface.

gradients of strain perpendicular to the measured surface. Displacements between horizontally arranged pairs of dots fixed to the beam's vertical surface were measured with a microcomputer-controlled video monitor. Digitized images of the dot positions prior to and after beam deflection were compared, and the distribution horizontal strains across the beam's vertical cross-section were calculated. Strain mappings in the vicinity of knot defects and of laminae of comparatively low elastic modulus were of substantially greater magnitude than predicted by simple elastic beam theory.

A Study of Load-induced Microdeformations within Wood-based Structural Members Using Optical Scanning Techniques

by

David C. Irving

A THESIS

submitted to

Oregon State University

in partial fulfillment of
the requirements for the
degree of

Masters of Science

Completed January 16, 1989

Commencement June 1989

APPROVED:

Signature redacted for privacy.

Dr. Phillip E. Humphrey
Assistant Professor of Forest Products in charge of major

Signature redacted for privacy.

Dr. Robert Ethington
Head, Department of Forest Products

Signature redacted for privacy.

Dean of Graduate School

Date Thesis is presented January 16, 1989

TABLE OF CONTENTS

LIST OF FIGURES

LIST OF TABLES

A STUDY OF LOAD-INDUCED MICRODEFORMATIONS WITHIN WOOD-BASED STRUCTURAL MEMBERS USING OPTICAL SCANNING TECHNIQUES

CHAPTER 1

INTRODUCTION

Lumber and laminated wood products have been used widely in structural applications for many years. Cost effectiveness and ease of installation are principal reasons for using these wood materials in preference to steel and concrete. However, the variability of wood forces the use of very conservative safety factors in design formulae to provide adequate structural reliability. In addition, assigned working stresses for structural lumber are quite constrained, and often based more upon statistical distribution data than a detailed knowledge of the material itself. This relatively high level of uncertainty results in inefficient wood utilization and design practices, and decreases the competitiveness of wood as a structural material. The realization of more efficient use of wood for structural applications depends heavily on our abilities to understand more fully and to predict accurately the mechanical behavior of wood members under load.

1.1 Background

The gross mechanical behavior of any structural member is governed by the organization and properties of the individual materials of which it is comprised. However, the high frequency and variety of irregularities within wood, such as knots, cross grain, and specific gravity variations, make it difficult to assess the influences that each material characteristic has on the mechanical properties of complete wood-based components. Nevertheless, relationships between these specific complex features in the material and overall mechanical performance of structural members must be established if wood-based products are to be designed and used efficiently. Stiffness and strength are the primary properties of concern in structural applications.

Measuring strain distributions in a loaded member is a quantitative means of discerning how the material's structure, and irregularities within that structure, effect gross mechanical behavior. In the same way, a numerical mapping of micromechanical behavior within specimens would be a direct approach to understanding how specific irregularities in wood structure influence overall mechanical performance. The experimental derivation of strain distributions or mappings at critical locations in wood-based members may provide a link between material structure and member performance. This interdependence is represented schematically in Figure 1.1. Numerical measurement of localized deformations that occur around defects, as well as at interfaces between materials of contrasting elasticities, has considerable potential for providing fresh insights into current elastic, inelastic, and fracture theories for wood.

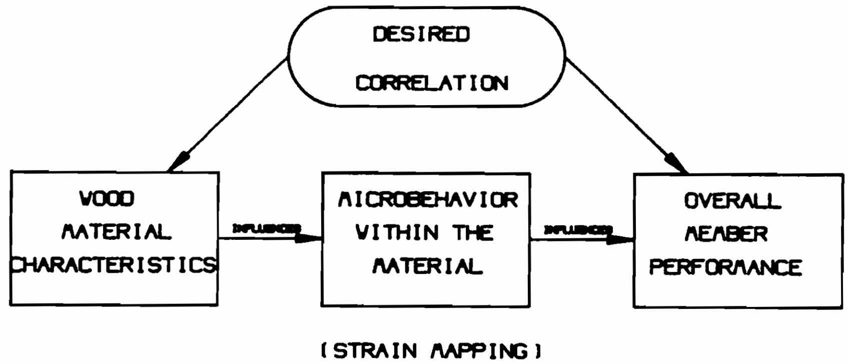

Figure 1.1 Linking role of strain mapping to correlate material structure to complete member performance.

1.2 Objectives of the research

Investigations of stress and strain distributions in the field of wood mechanics has been primarily confined to the development of models, particularly using finite element techniques, which provide complete stress fields in the vicinity of a specific material inhomogeneity (Cramer and Goodman, 1983). However, in developing these models, many limiting and unverified assumptions must be made about localized elastic properties and mechanical responses of the material. Confirmation of the modeling results with actual tests is necessary to determine the validity of the models and to pinpoint incorrect assumptions. There is presently a lack of reliable techniques for experimentally measuring strain or stress fields on test specimens in wood mechanics.

The experimental difficulty of strain measurement on wood specimens are two-fold. One factor is that dimensional instability and hygroscopicity (inherent in any woody substance) is not conducive to the use of most contemporary strain measuring devices. A second and probably more significant reason is that wood, unlike most other structural materials, is an anisotropic material in its basic form.

This three-dimensional variablilty of wood prevents direct inferences from being made about micromechanical behavior since strains can only be measured on the surface of the specimen, while unknown gradients of strain may extend perpendicular to the measured surface. Figure 1.2 illustrates this concept on clear wood material. As shown in the diagram, each thin member constituent will exhibit different mechanical behavior depending upon the orientation of earlywood and latewood bands, which have contrasting stiffness properties, with respect to the geometries of the members. As a result, the distribution of measured surface strains only relate to surface behavior (the outer two thin members) and cannot be used to infer internal behavior (the inner sections). In the vicinity of defects such as knots, internal strains are even more ambiguous. Thus, relationships between gross beam properties and surface strain and stress distributions is difficult to derive experimentally. Variability must be somehow drastically reduced in the transverse plane before gradients of strain in the third-dimension can be assumed to be minimal.

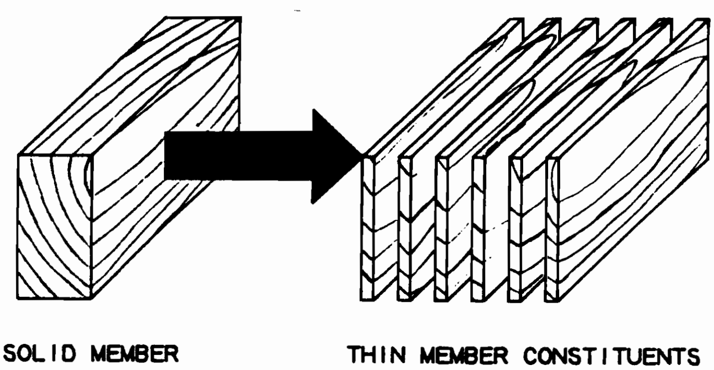

Figure 1.2 Demonstration of how wood's anisotropy prevents direct correlation of measured surface strains to internal strains.

The overall objective of the present research is to develop a technique that will minimize transverse variability in wood specimens such that measured surface strain data can be interpreted appropriately. In this way, specific characteristics of wood structure can be related to mechanical performance of the member directly. This should provide a reliable means for validating or refuting modeling data on stress and strain distributions in wood and wood-based materials, as well as being a useful tool to aid in the development of new structural composite materials.

Outlined herein, therefore, is a strain analysis technique which has been developed to considerably reduce the effects of variability in the third-dimension in wood such that surface characteristics and associated strains better represent overall behavior within the member. The method involves measuring surface strains on very thin laterally restrained bending members, which physically reduces third-plane variation. This direct approach is intended to simplify the analysis of strain and stress distributions in wood-based materials to two dimensions. Before going on to describe this approach in detail (Chapters 3 and 4), the need for the present research and the rationalle underlying the approach will be discussed in the context of the literature (Chapter 2).

CHAPTER 2

LITERATURE REVIEW

2.1 Grading and designing structural members: background

Wood is often described as an orthotropic material. This suggests that it exhibits differing mechanical properties in the directions of three mutually perpendicular axes; these are usually termed longitudinal, tangential, and radial directions. The general assumption, however, only has applicability in the absence of defects and if characteristics such as growth rings are not considered. Irregularities in wood, such as knots, interupt order in the arrangement of wood fibers and this leads to anisotropic mechanical behavior in those regions. As a consequence, stresses are distributed in a complex manner during loading, and directly effect mechanical performance (USDA, 1987). Attempts to establish quantitative correlations between specific defects and their influences on the mechanical behavior of structural members when simply loaded are rather speculative. Mechanical interactions are even less well understood when the more complex flexural mode is applied because of the simultaneous presence of tensile, compressive, and shear stresses (Price, 1967). The effects of material irregularities on the strength and stiffness of a flexed wood member depends upon their type, size, location, soundness, shape, and attendant slope of grain with respect to the neutral axis (Wangaard, 1950; Freas, 1962).

In an effort to minimize stress concentrations in beams, and thereby optimize performance, several wood-based structural products are designed specifically to distribute defects throughout the member.

Such is the case with Laminated Veneer Lumber and structural panel products. However, structural lumber and laminated beams are more susceptible to the detrimental effects of defects within them. Ensuring reliable strength properties in these structural products (especially dimension lumber) has historically been a difficult task. As with any structural material, the allowable engineering design properties must be either inferred visually or measured non-destructively. Stemming from a lack of conclusive experimentally-derived data on the influences of defects on beam stiffness and strength, empirical reasoning and statistical data continue to be the principal means for estimating these mechanical properties (NFPA, 1982). The following two sections describe contemporary methods for estimating lumber and laminated beam strength and stiffness for stress grade assignment.

To ensure safety in design, it is intended that the actual strength of at least 95 percent of the pieces in a grade exceed the allowable properties in that grade. Both Working Stress Design and Load and Resistance Factor Design methodologies therefore require that conservative estimates are made to overcome the wide property variations inherent among pieces within grades (Ellingwood, 1981).

2.1.1 Grading structural lumber

Visual criteria are predominently used to assign allowable stress grades to solid-sawn wood. Even machine stress-rated (MSR) lumber normally receives visual inspection before higher design stresses may be assigned (Bodig and Jayne, 1982; WWPA, 1980). Structural design values for visually graded lumber are currently derived by use of the strength ratio concept (USDA, 1987). A strength ratio is the hypothetical ratio of the probable strength of a piece of lumber with visible strength-reducing characteristics to the strength it would exhibit if those characteristics were absent. Strength ratios are usually expressed as percentages. An individual piece of lumber will often have several growth features which can affect strength properties. Only the characteristic which yields the lowest strength ratio is used as a basis to asssign a grade. Clearly, this approach does not account for the additive or interactive effects that certain characteristics may have on behavior.

Strength ratios for abnormalities of density and cross grain have been estimated empirically, whereas strength ratios for other growth characteristics have been obtained analytically. Design values for beams loaded in flexure are derived from clear wood values cataloged in ASTM D 2555 (ASTM, 1986a) which are modified by procedures specified in the ASTM standards D 2515 and D 245 (ASTM, 1986b, 1986c). Taking a knot defect as an example, this standard assumes that strength and stiffness property reductions are related to an effective reduction in the cross-sectional area of the member. The <u>basic expression</u> (USDA, 1987) which is used to determine the influence of a knot is:

$$SR = 1 - (k/h)^2 \qquad (2.1)$$

where: SR = strength ratio
K = knot size
h = face width containing the knot

Lumber stiffness values are derived by combining the assigned strength ratio value with cross-sectional dimensions of the beam. This procedure is described in ASTM D 245 (ASTM, 1986c). The clear wood average is multiplied by a "quality factor" which represents the reduction of modulus of elasticity associated with grade.

Itani and Fahety (1984), Aplin and Keenan (1977), and Galligan and Green (1980) concure that the current ASTM standards result in overly conservative assigned design values and that further research relating defects to performance could justify revisions in these standards as well as lumber grade reclassification. The strength distribution histogram shown in Figure 2.1 demonstrates the broad variability present within a particular stress grade. Although this paper does not specifically address derivations of material strength, this data was used to illustrate that a deeper understanding of wood mechanics is a requisite for more efficient material utilization. Incorporation of new knowledge in this area into grading criteria should reduce the variability of properties within grades.

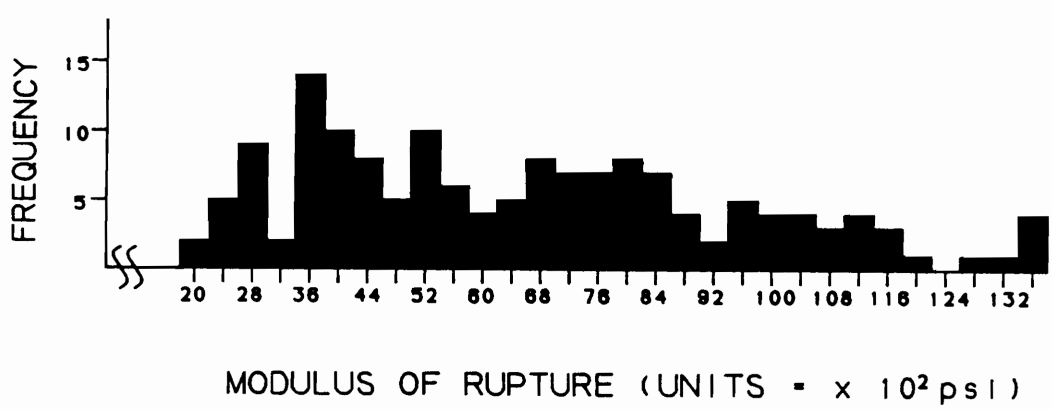

Figure 2.1 Frequency distribution of bending strength for a select structural grade (Fernandez, 1975).

2.1.2 Designing laminated beams

The inaccurate assessment of strength and stiffness values for lumber has serious consequences when relied upon in laminated beam design. Wide variations in the properties of each lamination can create complex interactions between laminations which, in turn, directly influence the mechanical behavior of the laminated system as a whole.

Design and manufacturing standards are dictated by the American Institute of Timber Construction (AITC) through a variety of specifications based upon the American National Standard ANSI/AITC A190.1 (AITC, 1983), as well as ASTM D 3737 (ASTM, 1986d) and ASTM D 2559 (ASTM, 1986e). Specific requirements have been made for lumber to be used in specific sections of the beam: 1) outer region under tension, 2) inner region under tension, 3) core, 4) inner region under compression, and 5) outer region under compression. Certain strength requirements also apply to the top and bottom laminae.

The design of laminated beams depends on an understanding of stress distributions in the member under load which, in turn, rests upon the combination of laminations of different flexural stiffnesses used in their fabrication. In addition, knots and slope of grain must also be accounted for, as their presence in the beam section also influence the beam's properties. These two factors are assumed to not be interactive, with the lower of the two determining the properties. In most cases, knot defects are the limiting characteristic (AITC, 1983). Two different approaches are used for estimating a laminated beam grade. The particular method employed hinges upon beam depth.

The bending strength of deep beams has traditionally been based upon a reduction of the flexural strength of clear wood by means of a factor which takes into account the particular lamination grades in the lay-up and the knots within each lamination (Freas and Selbo, 1954). In this approach, two moments of inertia are computed for the beam cross section: Ig, the gross moment of inertia, and Ik, the sum of the moments of inertia for the knot areas within a prescribed beam length. The strength reducing factor is expressed as a function of the Ik/Ig ratio. The method has been widely used, but has not received strong experimental support in studies by Fox (1978), Bohannan (1966a), and Moody (1977).

The strength of shallow beams has typically been predicted using a strength ratio concept adapted from the ASTM D 245 standards, which is based upon the reduction of the section modulus due to knots and other defects. Although this method predicts shallow beam strength more closely than the Ik/Ig technique, unsatisfactory correlations have been obtained by Moody and Bohannan (1970) and Marx and Moody (1981a, 1981b).

The resounding conclusion of researchers specializing in the design of laminated beams is that a better understanding of relationships between various wood characteristics and performance is required before significant improvements in performance and reliability may be achieved. Specific interactive relationships between laminae, with or without defects, must be established analytically (Marx and Moody, 1981a). This need is evident in Figure 2.2 which shows a distribution of strengths among a sample of laminated beams designed for the same grade.

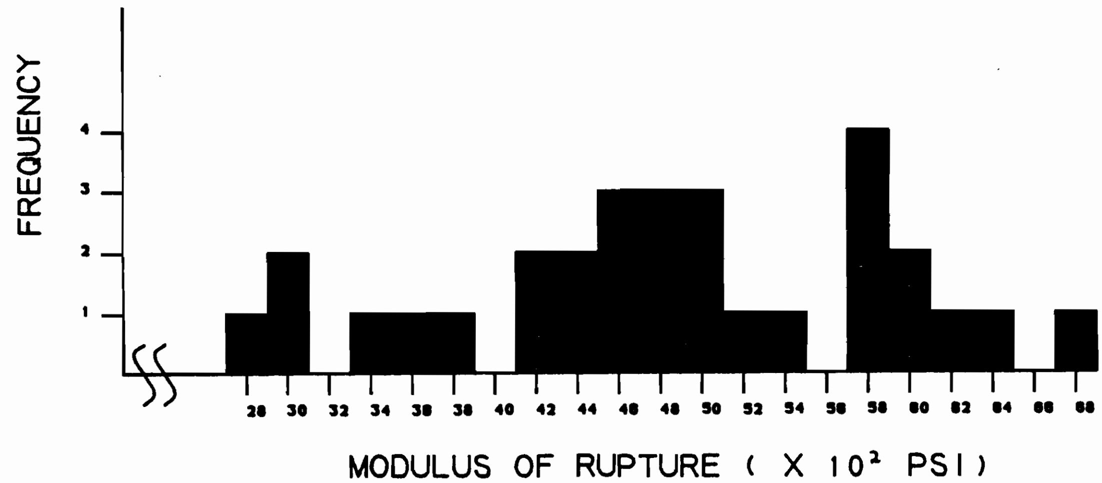

Figure 2.2 Frequency distribution of bending strength for a 20-F grade Douglas-fir laminated beam (Fox, 1978).

2.1.3 Direction of research efforts

The intent of this paper is to develop techniques which may aid in improving our understanding of the correlation between visible characteristics of wood structure and material properties. Cramer and Goodman (1983) contend that reliable predictions of wood properties require a knowledge of local strain and stress conditions that occur when structural members are loaded. Such information is particularly important in the vicinity of irregularities within the member. An improved understanding of how the distributions of stress and strain influence overall mechanical performance of members may lead to a reevaluation of contemporary lumber grading rules and laminated beam design methodologies.

Current methods of strain and stress analysis for material evaluation generally fall into two categories: (1) numerical modeling techniques, and (2) experimental methods (Weathers, et al., 1985). Numerical modeling methods generally involve numerical simulation of material behavior under load. Before such simulation models are formulated, a range of hypotheses and assumptions must be made about the material and its properties. The quality of any model depends upon the sophistication and accuracy of the theories upon which it is based. Experimental methods typically involve direct measurement of stress or strain distributions that occur within specimens as they are loaded and deformed. The latter are certainly more direct approaches, but present experimental difficulties when applied to wood materials. The intent of both approaches is to establish a clear understanding of how mechanical properties are influenced by the anatomical structure of the material. Figure 2.3 outlines the interdependencies among these disciplines. The following two sections (2.2 and 2.3) provide an historical perspective on theoretical and experimental methods of quantifying stress and strain distributions in structural members as they deform.

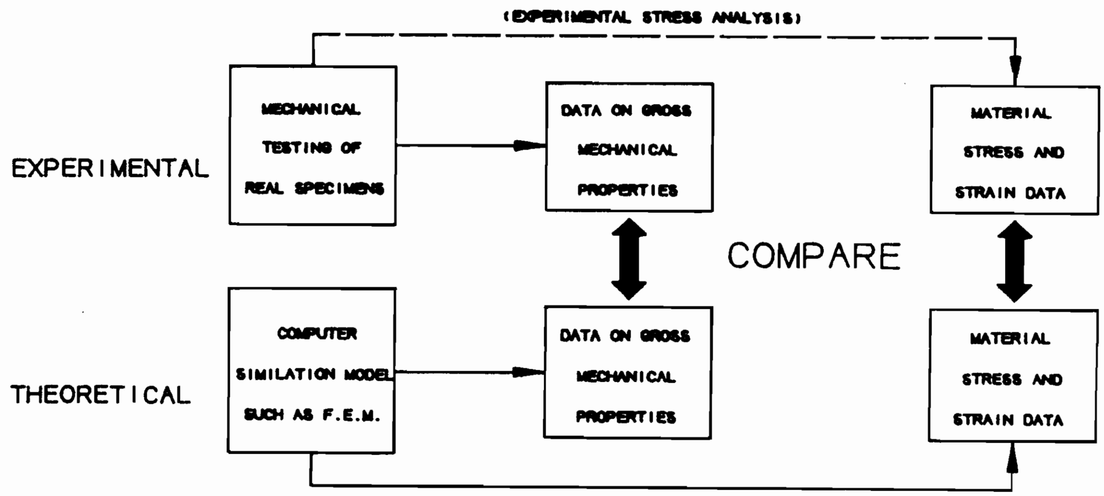

Figure 2.3 Interdependent relationship between theoretical and experimental wood mechanics research. Dashed lines indicate an absent but essential component.

2.2 Modeling wood behavior

Numerical modelling of the mechanical behavior of wood-based structural members can be conveniently divided into two distinct areas. These may be termed (a) statistical and (b) material simulation. Each will be briefly considered in turn.

Statistically-based modeling:

Statistical modeling provides a rational and consistent way to deal with the uncertainties of wood properties. The method depends upon statistical information relating load and resistance of wood materials with various defect types. This approach seems to mesh well with upcoming reliability based design procedures (Goodman and Criswell, 1983) and in-grade testing programs. Work by Liu (1980), and Suddarth and Galligan (1978), has demonstrated the practicality of the approach. However, statistical modeling does not provide the deterministic information on material behavior critical to efficient utilization and design practices.

Material simulation modeling:

Material simulation is an approach which has demonstrated greater usefulness for quantifying how particular material traits affect gross mechanical behavior. Refinement of finite element techniques and the development of new high speed computers has further augmented the usefulness of this strategy. The value of material simulation models lie in their ability to provide stress and strain values at any location in a loaded structural member (Cramer and Goodman, 1983).

The success or failure of a simulation algorithm is critically dependent upon the empirically and theoretically-derived assumptions made in setting up the model (Pagano, 1978). The accomodation of boundary conditions is typically accomplished by the development of theories based on experimental tests of similar materials, and can be incorporated into the model through a variety of means. Zakic (1983) has listed some common generalizations of wood mechanical behavior in bending that are often used in models. These include:

(1) Knots are more detrimental to tensile than to compressive strength.

(2) Wood with knots fails suddenly without warning in tension.

(3) Defect-free wood beams fail first in the compression fibers, preceeded by large plastic deformations.

(4) The modulus of elasticity in tension and compression can be taken as the same.

(5) Stress at the proportional limit in tension is about 2-2.5 times that in compression.

(6) The tensile strength is 2-3 times that of the compressive strength.

(7) The proportional limit in compression occurs at a strain of approximately 2.5 x 10-3 in/in.

(8) The difference between the behavior of wood in tension and compression in the elastic-plastic range results in a shifting of the neutral axis towards the tension surface.

Orthotropic elastic and fracture properties are assumed to be uniform, using parameters from work by researchers such as Bodig and Goodman (1973) and Barrett and Foschi (1977) respectively. Development of more specific fracture criteria for use in models has been investigated with reasonable success by Cramer (1984) and Pugel (1986).

Other assumptions for modeling relate to the physical orientation of fibers and defects within the material. A geometric method of prediction for localized grain deviations around a knot has been developed by Phillips, Bodig, and Goodman (1981) which relates grain lines in the vicinity of a knot to streamlines of laminar fluid flow around an elliptical or circular object. The applicability of the technique is, however, limited due to the wide variation of grain in real knots (Tang, 1984). The potential pitfall in making these broad assumptions about wood structure and behavior is that they frequently oversimplify the material to an extent which invalidates the results.

Many computer simulation models for wood mechanics have been developed using the finite element method (FEM). This analytical method involves replacing the actual continuum by an assembly of discrete, or finite, elements connected together at their corners or "nodes". The elastic and inelastic properties of the finite elements can be specified to duplicate the material properties of actual members. Evaluation of the quality of the analysis is often accomplished by comparing gross theoretical and experimental properties. Typically, the reliability of stress predictions are determined by checking the convergence of model-derived values as finer meshes are used (Cook, 1981). Models have been created to represent the behavior of both solid wood and laminated beams with and without defects such as cross grain and knots. Pioneering work using FEM was conducted by researchers such as Maki (1968) who adapted the technique to study orthotropic material behavior. This was later refined by Al-Dabbagh <u>et</u> <u>al.</u> (1972). Etherington <u>et</u> <u>al.</u> (1972), Keenan and Selby (1973), and Swift and Heller (1974) expanded modeling capabilities to enable computation of layered laminated beam behavior. Reasonably successful simulations of the mechanics of wood which include defects such as cross grain have been accomplished by Silverman (1980) and Foschi and Barrett (1980). However, additional work by Zakik (1983) and Cramer and Goodman (1983) demonstrated the need to incorporate shearing effects and more exacting elastic parameters. This resulted in better correlations between predicted and experimentally derived stiffness and strength values.

Stemming from a knowledge that strength properties of wood are intimately associated fracture mechanics (Schniewind and Pozniak, 1971; Barrett and Foschi, 1978), interest in recent years has been focused on the analysis of stress concentrations near defects and failure modeling. Tang (1984) has investigated the effects of size, shape, location, orientation, and material properties of knots on stress concentrations in wood members. However, this work has not yet been verified by experimental means. Models which draw on both FEM and fracture mechanics were developed by Cramer (1984), and Cramer and Goodman (1986). These model progressive failure mechanisms that may be observed in wood members. Although computer simulations of wood mechanics provide reasonable predictions of overall member stiffness and strength, the stress and strain data obtained in a given model is difficult to verify experimentally. This fact highlights the importance and need for a direct strain measurement technique for mechanically tested wood specimens.

2.3 Experimental measurement of wood behavior during beam flexure

Clearly, a knowledge of the distribution of stresses and strains that develop within a member as it is loaded is critical to our understanding of the influences that various anatomical irregularities have on gross mechanical behavior. There are a broad variety of techniques which have been used with considerable success in measuring planar surface strains in materials. The following methods have been used (Weathers, et al., 1985):

-holography	-Moiré
-speckle interferometry	-photoelasticity
-double exposure interferometry	-strain guages
-extensiometers	-brittle coatings

Although these techniques have been widely accepted and used for evaluating metallic, plastic, and ceramic materials, the application to wood has been difficult because of the porous, anisotropic, hygroscopic, and dimensional instability of the material.

Most investigations involving experimental stress analysis of wood were performed in the 50's and 60's, before the advent of finite element modeling techniques. FEM was rapidly adopted in place of experimental stress measuring methods because of the much greater ease in obtaining crucial stress data. However, as stated before, model-derived stresses cannot be relied upon without verification with experimental data. At the present time, only photoelastic, strain guage, and brittle coating methods have been used to study wood materials to any large extent. The relative usefulness of each of these three methods is considered next before going on to introduce the laminar approach developed in the present research.

2.3.1 The use of photoelastic methods for strain measurement

In this technique, clear sheets of plastic with a reflective cement or coating on one side are bonded to a prepared wood surface. When the photoelastic surface coating is strained and viewed under polarized light, colored birefringement patterns appear which correspond to a definitive strain level (Budynas, 1977). Schniewind (1963) used the method to quantify the formation of checks in wood during a drying process. The method was also used by Stieda (1964, 1965) and Price (1967) to measure strains in the vicinity of defects. Takahashi and his co-workers (1964a, 1964b, 1965, 1966a, 1966b, 1966c) have also conducted extensive experiments using this technique with wood. There has been a general concensus made by all of these researchers regarding the use of photoelastic techniques. Apparently, it is very difficult to bond the plastic membrane to wood without causing residual birefringence from surface irregularities and moisture effects. These can induce considerable error in strain resolution (Price, 1967).

2.3.2 The use of resistive strain guages for strain measurement

Electrical resistance strain guages have probably been used more often than any other method for stress analysis problems in wood. A strain guage consists of a grid of strain-sensitive metal foil which is bonded to a flexible plastic backing material. The guage is, in turn, bonded to the surface of the specimen. When the specimen is stressed, surface strains are transmitted to the foil grid. Resultant changes in electrical resistance of the grid material are proportional to the strain (Budynas, 1977). Youngquist (1957) published a critical report on using strain guages to measure microdeformations within wood. Other researchers (Radcliff, 1955; King, 1957; Asano and Tsuzuki, 1960; Maki and Kuenzi, 1965) have developed refinements and studied the limitations and usefulness of strain guages for measurements on wood. The principal advantage of strain guages is their ability to measure the average strain over a small guage length. However, the presence of growth rings, surface roughness, and absorbed moisture can limit the accuracy of measured strain data (Price, 1967; Youngquist, 1957). Resistance to deformation offered by the backing of the strain guage itself may also detract from the accuracy of the method on more highly elastic materials such as wood.

2.3.3 The use of brittle coatings for strain measurememt

This method involves the application of a brittle lacquer coating to the surface to be studied. When subjected to a positive strain (tensile deformation), the rigid lacquer will develop cracks oriented perpendicular to the direction of the largest normal strain. The number of cracks per unit length may be used to provide an indication of the magnitude of the strain (Budynas, 1977). Compressive strains must be determined by a more complicated procedure. Brittle coatings have the advantage of obtaining principal strain trajectories directly.

A limited number of investigators (Hatayoma, 1960; Ickovic, 1963) have used this method on wood. They found that correct application of lacquer to the wood surface is a rather tedius operation and difficult to control. Cunningham and Yavorski (1965) studied the strain field in a glue block shear specimen using brittle lacquer. However, the brittle coatings have been most useful as a qualitative indicator of tensile strains in wood subject to tensile stresses (Fritz, 1967). Unfortunately, the capabilities of brittle coatings do not extend to the study of flexural behavior.

2.3.4 A thin member approach to strain analysis

One of the principal shortcomings of the preceeding experimental methods lies in their inability to provide data on strains that occur beneath the surfaces of the body as it is deformed. Information on internal strains is, however, important when studying anisotropic materials like wood since the influence of defects must be quantified three-dimensionally. A need to overcome this deficiency inherent in two-dimensional (surface) measurement techniques has been expressed by experimental stress researchers Price (1967) and Fritz (1967), as well as numerical stress investigators Cramer and Goodman (1986). Ostman (1985), in studying the behavior of bolted wood joints, has developed a wood laminar technique which may provide one possible remedy to this problem. This research involved using thin wood wafers as test specimens to observe joint failure mechanisms which are hidden from view in full width members. Use of this principle may enable the three dimensional problems noted by the forementioned researchers to be significantly reduced; it could provide a viable means to relate measured strains to localised wood structure.

The approach outlined in this paper draws on the work of Ostman (1985), as well as the experiences of previous researchers who have performed experimental stress analyses on wood. This paper describes a new technique for direct strain measurement which can be used as a means of verifying and complimenting the contemporary numerical simulation (FEM) approaches. It will be fully described in the chapters to follow.

CHAPTER 3

PRELIMINARY STUDIES OF MICRODEFORMATIONS IN FLEXED SPECIMENS

3.1 The thin wafer technique outlined

Before embarking upon the principal research of this project, some preliminary investigations using thin wafer techniques were conducted to enable an appropriate research strategy to be planned. Research performed by Ostman (1985) demonstrates the potential of using thin specimens for analysis of large structural systems. The so called "laminar technique" involved the testing of specimens specially cut to a thickness of 0.030" thick which were restrained between glass plates. This was used with considerable success to study the behavior of bolted joints loaded in tension. Compressive deformations and crack propagation could be readily seen with a bright backlight and thus enabled failure modes to be sequentially identified during loading to failure.

In the present study, which concerns the behavior of beams, it was felt that the approach could be used to minimize the effect of variability in the third-dimension (perpendicular to study plane). This could enable the interaction of features clearly identifiable on the surface of specimens to be related to behavior under load. Many aspects of Ostman's technique were duplicated in this preliminary work, with the hope that compressive, tensile, and shear deformations and failure modes could be observed. Visualization of strains during the testing process appeared to be a simple means to at least qualitatively investigate the strain field within bending members.

The apparatus utilized plexiglass plates held in place with pneumatic pistons to offer continuous lateral restraint to parallel sliced Douglas-fir wafer beams measuring 1" in depth by 16" in length. The apparatus is shown in Figure 3.1. Some specimens were radially sliced from clear material while others were tangentially sliced from material which incorporated a knot defect. A bright light source was placed behind the specimen to aid in exposing changes in its microscopic structure during bending (see Figure 3.2). Load was applied by specially manufactured indentors which passed through slots machined in the plexiglas supports. The whole arrangement was mounted on the universal testing machine (Instron).

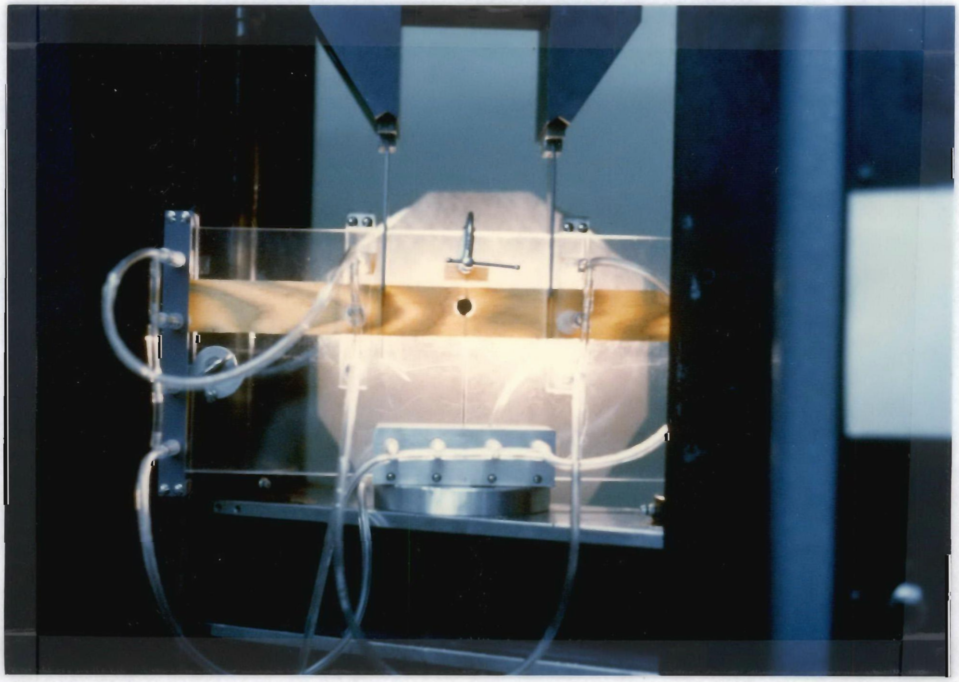

Figure 3.1 The testing apparatus used for evaluating flexural behavior of wafer specimens

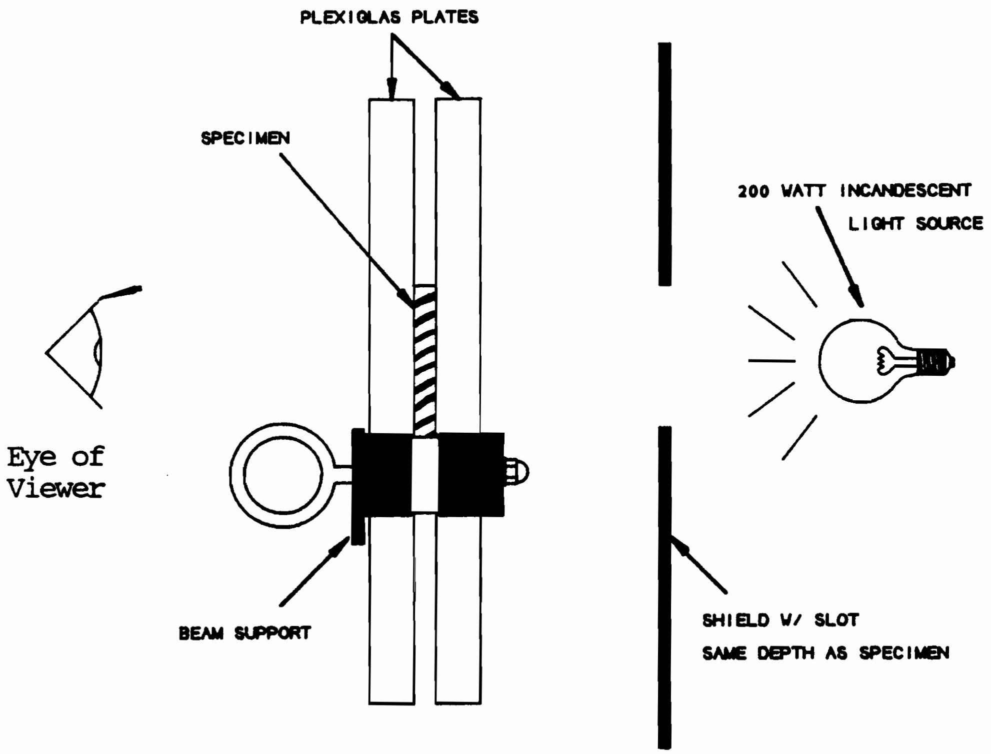

Figure 3.2 The arrangement for illuminating the specimen for qualitative observation of strain during a flexural test

The principal conclusions drawn from this preliminary investigation were as follows:

(1) Deformations within the material only became evident after failure was initiated. No microscopic deformations prior to failure could be detected with the naked eye.

(2) The orientation of the wood structure within the wafer (radial or tangential) appeared to influence the ultimate strength, stiffness, and mode of failure. The highly irregular grain patterns exposed on the surfaces of the tangentially sliced specimens appeared to be a major drawback to studying behavior in that orientation.

(3) Lateral instability of the thin specimens was not sufficiently overcome by this preliminary testing arrangement.

(4) There was a high level of uncertainty regarding the localised frictional restraint acting between the specimen and the plexiglas plates. This made it difficult to achieve accurate load measurement.

3.2 Outline of a viable approach

Since elastic and inelastic strains could not be observed in the thin specimens during flexure, the need for instrumentation to determine strain fields became evident. This subsequently became a major focus of this research. In addition, it was apparent that the plate-type lateral restraint used in the preliminary study was inadequate. If a wider beam could be studied, then the need for restraint over the entire specimen surface would be avoided, and strains could be measured on the surfaces without the interference of plexiglass or glass surfaces. Clearly a disadvantage of using wider specimens is the associated increase in variability. Attempts were therefore made in ths preliminary investigation to determine the effect of width on the mechanical properties of beams loaded in flexure.

Specimen width effects

The effect of member size on mechanical properties has been quite extensively considered in the literature. Application of simple beam theory would suggest a linear correlation of beam stiffness and strength with beam width. However, Bohannan (1966b) measured the effect of specimen size on bending properties of wood members, and has shown that apparent constituent material properties inferred from flexural tests increase with decreasing specimen size. A theory proposed by Weibull (1939) suggests that a higher statistical probability exists that a region of low strength will occur in a member of large volume than a member of small volume. A region of low strength will, in turn, reduce bending stiffness and strength. These effects are most readily apparent and most easily interpreted when considering variations in beam width (rather than depth or span).

The effect of beam width on inferred modulus of elasticity (MOE) was investigated in the present study by repeated non-destructive flexure of beams followed by incremental thickness reduction. By horizontally laminating three close-grained and clear pieces of Douglas-fir together to form each specimen, variability across the width of the beam was kept to a minimum. The test members were loaded sufficiently to enable accurate stiffness measurements to be made but well below the proportional limit to avoid damaging the specimen during the testing sequence. Figure 3.3 shows a plot of the averaged MOE values obtained for the beams tested.

The principal conclusion drawn from this study is that apparent material MOE increases proportionally with a decrease in specimen thickness. The presence of a consistent relationship implies that size effects may be corrected for directly if so desired. This is important when attempting to relate thin beam behavior to that of full size specimens.

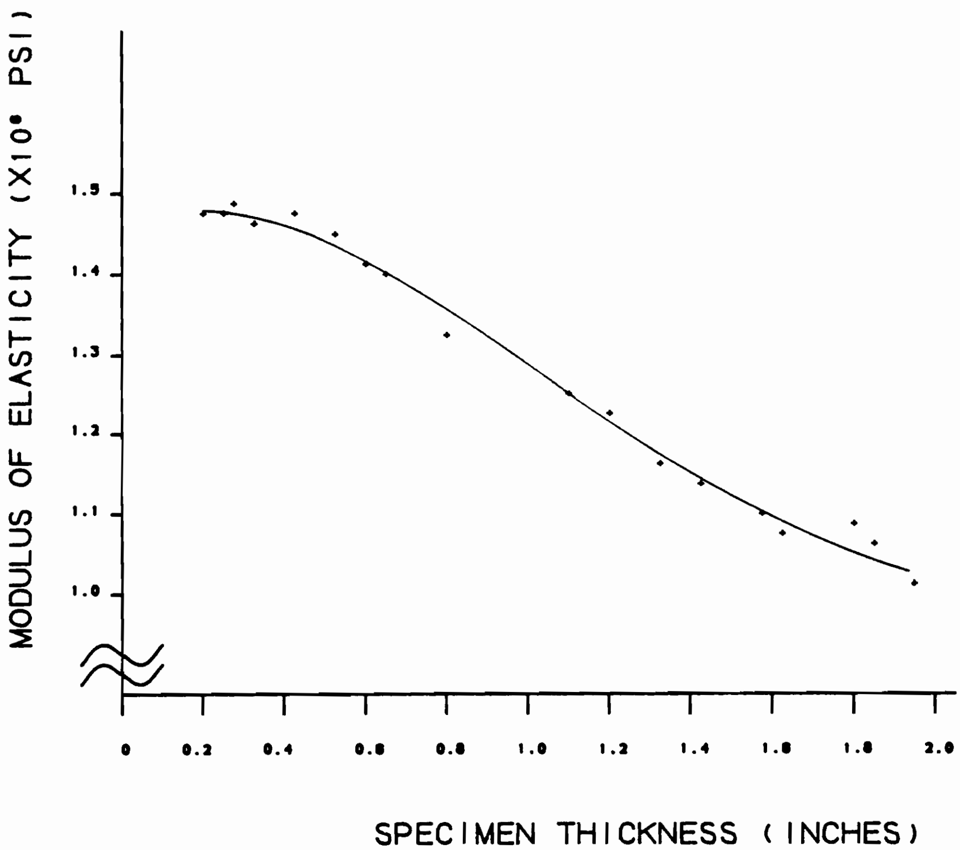

Figure 3.3 The measured effect of beam thickness on apparent MOE (average of four Douglas-fir specimens)

Selection of an appropriate beam thickness for the present research hinges upon several factors. An increase in width of the test beams clearly increases lateral stability, the proportional impact of certain surface characteristics diminish, and closer correlation with full size behavior may be attained. Disadvantages of increasing beam thickness are that deformations due to specific material characteristics become less identifiable and may be less easily related to features visible on the surface. It seemed that a thickness of approximately 0.25 inches would provide the advantages of a thin member and yet allow non-continuous lateral restraint to be used.

Material organization

Clearly, interpretation of behavior displayed on tangentially cut surfaces is dificult. Figure 3.4 demonstrates how variability in the transverse plane is affected by the geometry of the specimen. This preliminary work revealed that the benefits in studying thin members are most apparent when examining the radial face.

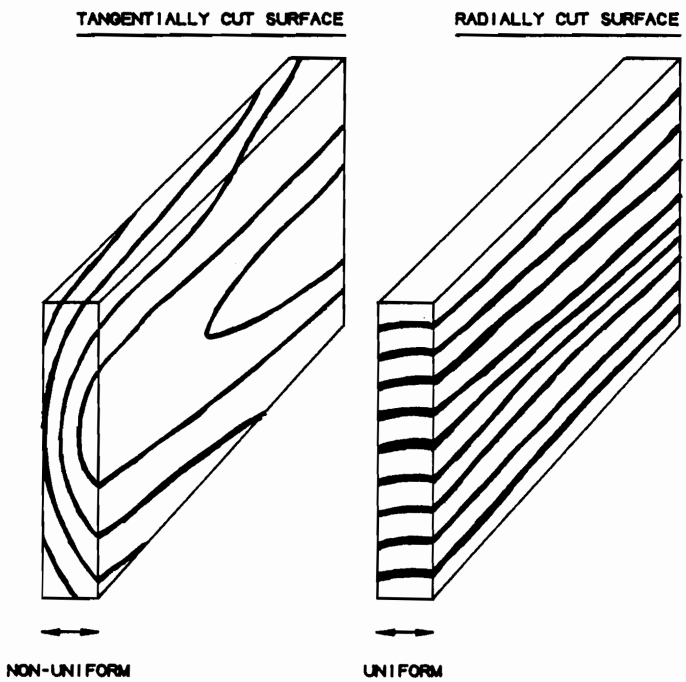

Figure 3.4 A comparison of tangential and radial orientations for uniformity across the width

The testing approach

As no visual qualitative observations of strain could be made using the backlighted technique described here, an alternative approach was necessary to measure surface strain. This strain measuring method must not interfere in any way with the bending properties of the wood members, especially since thin members are to be studied. The need for rigid support of the specimen has already been identified. Other requirements of the testing apparatus include the provision of supports which can provide lateral stability to the thin beams while under load. Lateral supports should be adjustable and induce minimal friction. An unobstructed and easily accessed surface upon which to make strain measurements is desireable. It was with these issues in mind that the technique described in the next chapter was devised and evaluated.

CHAPTER 4

EXPERIMENTAL METHOD

4.1 Introduction

The objective of this paper is to devise methods which can establish relationships between the structure of load bearing members and their mechanical performance. Regions in the vicinity of defects exhibit anisotropic behavior which implies that measured surface strains cannot be used to infer internal behavior. The approach undertaken here involves modification of the normally adopted testing sample. The analysis is reduced to a two dimensional case in which useful inferences can be made from mapping strains on the surface of narrow beams. Development of the technique focuses on three primary aspects:

(1) The design of an apparatus which can adequately test narrow beams in flexure while retaining lateral (in-plane) stability.

(2) The development of an appropriate method to measure surface strains. This must not influence the flexural behavior of the thin beams.

(3) Integration of (1) and (2) above into a technique which may be used to evaluate wood-based materials in which wood structure can be related directly to mechanical behavior.

The sections which follow address goals (1) and (2) in terms of system design, and goal (3) in terms of experimental methodology.

4.2 Design of the testing apparatus

Several methods can be used to induce bending forces in a semi-rigid beam. Three of the most common loading modes are termed moment-couple, two-point, and third-point. The resulting moment and shear diagrams from each of these is shown in Figure 4.1. Bodig and Jayne (1982) maintain that the effects of material inhomogeneities on mechanical properties is best studied in regions of the beam which are subject to constant bending moment and devoid of shear. Two-point loading, which is the typical testing method for small sized specimens specified in ASTM D 143 (1986g), does not provide this desired constant bending moment. Moment-couple loading has the disadvantage of being difficult to achieve experimentally without a complex apparatus. The third-point loading condition appeared to be the appropriate choice because it provides a constant bending moment along part of the beam and does not involve specialized testing equipment. The ASTM standard D 198 (1986f) describes appropriate reaction bearing areas and degrees of freedom for this configuration, and was useful for designing the present apparatus. The general loading configuration is shown in Figure 4.2.

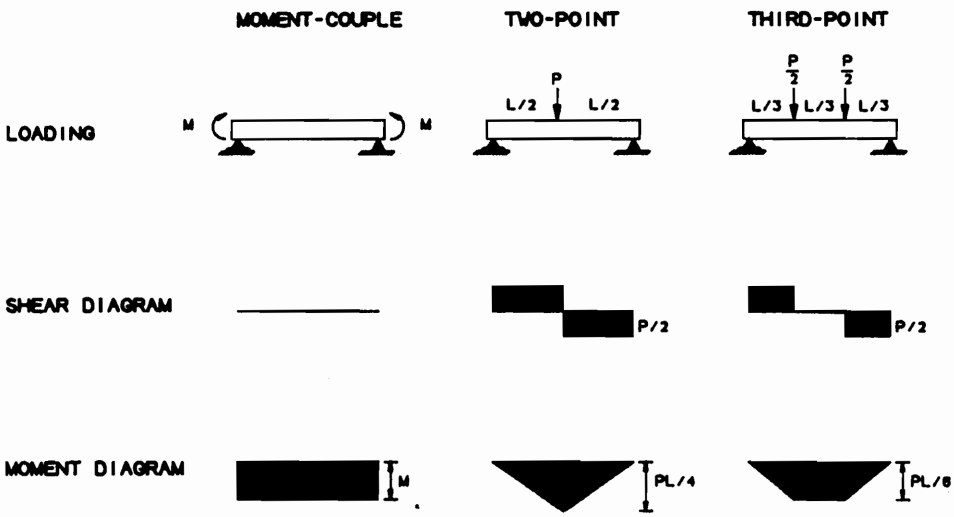

Figure 4.1 Three loading configurations for imposing beam flexure

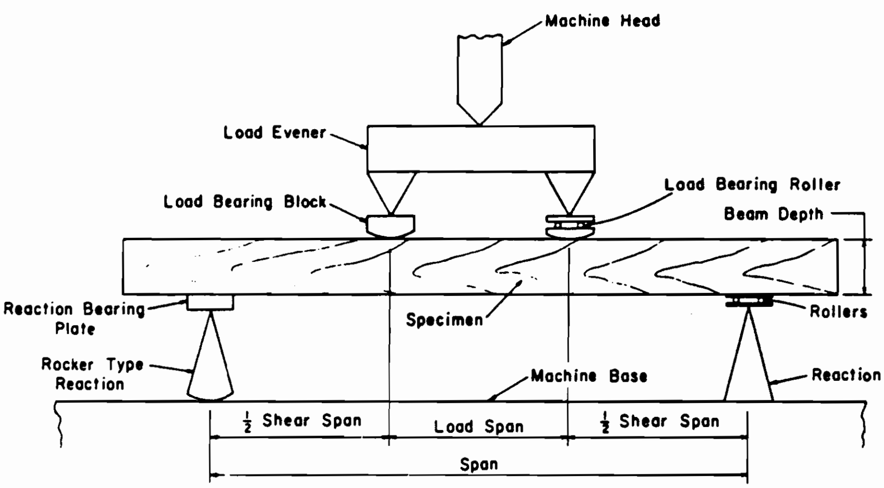

Figure 4.2 ASTM bending test of lumber

4.2.1 Load head design

The load head, which impart the load to the beam, were designed in accordance with the ASTM standard. To eliminate high stress concentrations at points of contact between the beam and bearing blocks, a radius of curvature on the blocks of at least two times the beam depth is recommended. Therefore, a radius of six inches was machined onto the aluminum load bearing blocks to minimize contact point stresses in the beams to be tested, which were to be less than three inches deep. The blocks were of sufficient width to contact the full beam width of 0.25 inches and designed to freely rotate on a horizontal pivot perpendicular to the span. Small tension springs were used to keep each block in alignment when not loaded. Rigid stainless steel bars linked the bearing blocks to a horizontal load evener. These could be adjusted to provide the desired third-point loading span. This was attached to the load cell via a hinge connection which allowed even load sharing among the two indentors to be achieved. The load cell was bolted to the testing machine frame. Figure 4.3 illustrates the entire load-imposing apparatus.

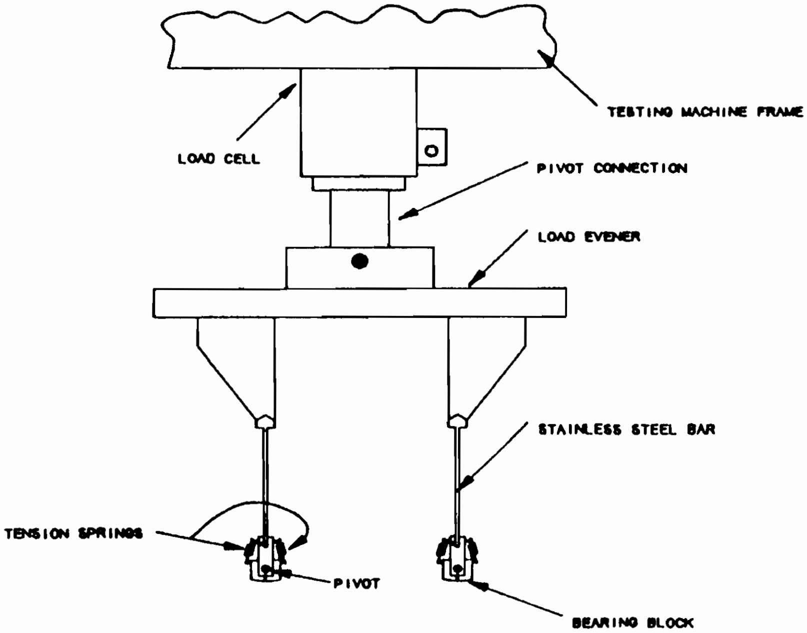

Figure 4.3 The indentor apparatus

4.2.2 Design of the foundation for support of the test beams

Metal bearing plates upon which the beam rested were designed with sufficient bearing area to prevent damage to the beam at the point of contact. With this and the small specimen size in mind, one inch by one inch plates were sufficient. Needle bearings were installed below one of the support plates to allow unrestrained displacement of the beam along its length as deflection progressed. The plate mountings were also hinged to enable small rotations of the beam ends to be accomodated. Reaction plate surfaces were kept horizontal with a tension spring to facilitate the setting up of specimens for testing. A slide and locking mechanism was used at the pillar base to allow adjustment for span length, and was housed in a channel within the base of the apparatus. A 45-inch long aluminum I-beam provided a sufficiently rigid foundation for testing beams up to 42 inches long. This I-beam base was bolted to the vertically acting piston of the servohydraulic testing machine. The support apparatus was designed to accomodate the testing of a broad variety of beam sizes, although this investigation only involved one size. A diagram of this beam support system is shown in Figure 4.4.

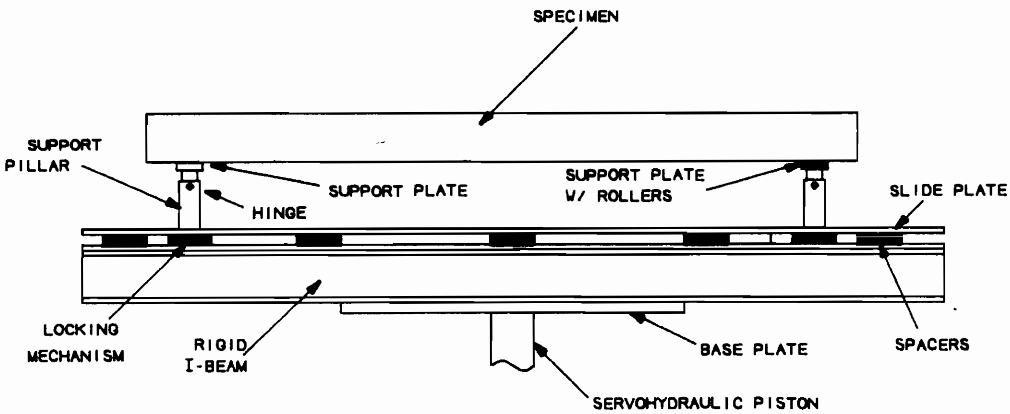

Figure 4.4 Beam support system

4.2.3 The provision of lateral support to the beam

The need for a non-continuous means of maintaining lateral beam stability has already been identified. To minimize, and yet be able to monitor, frictional restraint of beam deflection by the supporting devices was also a requisite. Supporting pillars were equally spaced at strategic locations along the beam length. Two possible approaches to controlling beam buckling with such an arrangement of pillars could be adopted. In the first, pairs of restraining struts lying on either side of the beam could be rigidly clamped in place with a separation between them very slightly greater than the beam thickness. Frictional effects are difficult to quantify when using such an approach because, as beam loads increase, variable and increasing lateral buckling forces act against the struts altering the frictional drag against the beam. A more viable alternative is to apply a constant restraining force to the sides of the beam via the struts. In this case, frictional forces in the system are held constant regardless of how near the beam is to buckling. If the laterally unstable beam imposes forces in excess of those imparted by the struts, the system will become unstable and buckling will occur. In this extreme situation, the struts would move apart. This catastrophic situation will not be reached if beam loads are kept within calculated limits of stability when accounting for the restraining effects of the struts. This constant force approach was most suitable for this application.

One side of each pair of restraining bars was fixed, while the other was hinged at one end. Each of the fixed struts were rigidly attached to a strait aluminum bar which extended along the length of the appartus base. In this way, the fixed restraints maintained longitudinal alignment of the beam. Each of the hinged struts was attached to a block via a pivot, which could slide freely perpendicular to the beam face. Independent adjustment of each strut enabled small irregularities in beam thickness to be accomodated. The movable block was locked in place by tightening a machine screw. Small double-acting pneumatic pistons linked the free ends of each hinged strut to the top of each rigidly mounted strut. This was achieved with specially made pivoting connections. With the pistons and piston rods in place, the struts flush to the beam surface, and the hinged strut base blocks locked into position, a controlled pressure could be applied to the beam surface as shown in Figure 4.5. The amount of force imposed on the beam surface may be adjusted by regulating the air pressure supplied to each of the pistons. An air regulator was used to control the air pressure diverted to all pistons simultaneously. A toggle valve triggered the double-acting pistons. The open position released the beam from the restraints.

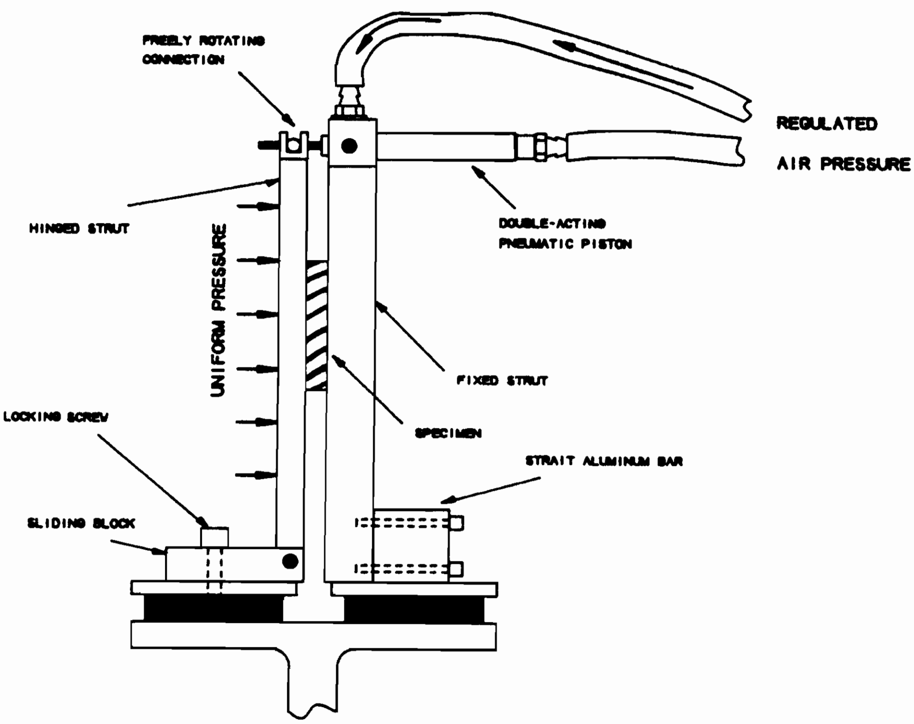

Figure 4.5 Side view of a pair of lateral supports acting on a beam

Six pairs of struts were used and they could be spaced along the length of the beam in one inch increments. The entire lateral restraint system is shown in Figure 4.6.

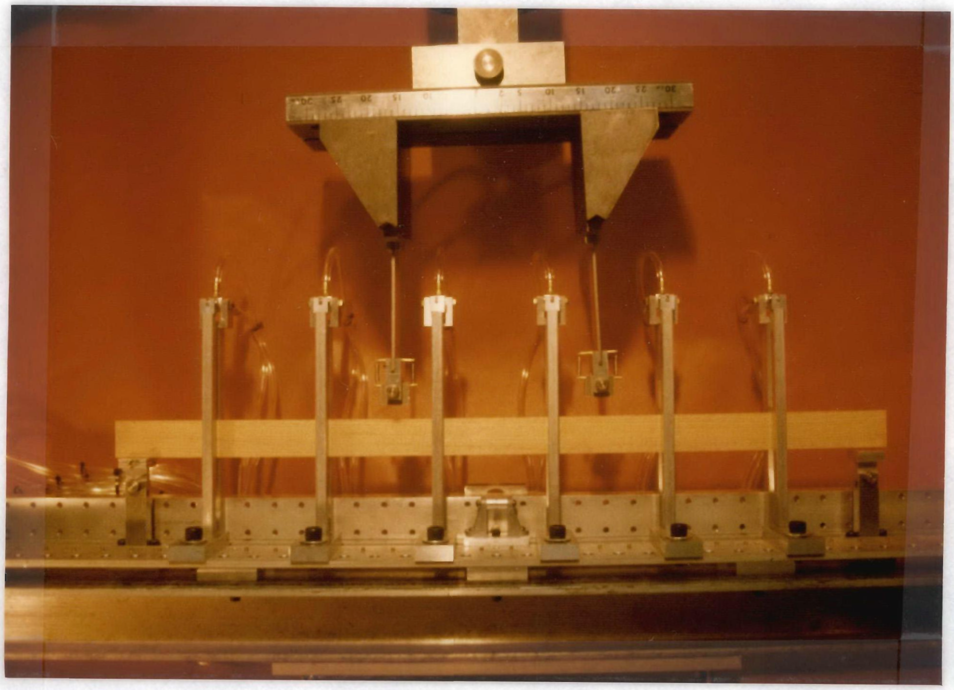

Figure 4.6 Photograph of lateral support system

4.3 Strain measurement on the beam surface during deflection

A number of methods for measuring strains on the surface of bodies as they are deformed have already been discussed (Chapter 2). This particular project, however, imposed certain limitations on the applicability of these existing technologies. First of all, surface irregularities and moisture effects in wood materials present problems not commonly encountered in classical experimental strain analysis. Secondly, the thin member approach warrants special attention to the strain monitoring method to avoid altering the sensitive behavior of the thin beams. A non-contacting method to monitor surface displacements was therefore required. It was with this particular need in mind that an appropriate strain measuring technique was developed.

4.3.1 Selection of an appropriate measuring technique

Photoelastic, Moiré, and brittle coating methods of strain measurement involve coating the test specimen's surface with some form of plastic film. These methods are not suitable for studying thin wood members because of the potential influence that the coating may have on the mechanical behavior of the system. Strain guages have the disadvantages of being unreliable on wood materials, and allowing only a limited number of points to be monitored in close proximity to each other.

Work by Chu and his coworkers (1985), as well as Peters and Ranson (1982), demonstrated the potential of computer vision systems for measuring strain fields. Their method made use of an image scanner interfaced with a computer which stored laser speckle patterns, first for a reference objective and then a deformed configuration. Data for the deformed images were numerically correlated with those of the reference image to enable surface displacements to be measured. Although their specific technique would not be easily applied to the study of wood materials, the principle of measuring surface displacements with a vision system seemed viable. Black dots, which contrast with the background surface tone of wood, can be used in a similar fashion to the laser speckle patterns of Chu et al. This simplified approach involves measuring how dots attached to the specimen's surface change position relative to one another as they travel with the moving fibers.

Due to the natural variation associated with images of biological materials such as wood, dots which contrast sharply with the features on the background surface are necessary. An initial grey-scale image is reduced to a binary one (black and white) during the first stage of raw data interpretation. Provided the dots are black and the background sufficiently light-colored, the scanned field may be partitioned to an array of black dots (blobs) on a white background. After partioning, spacial coordinates of the blobs may be analysed to compute relative displacement values. These are tasks are shown schematically in Figure 4.7.

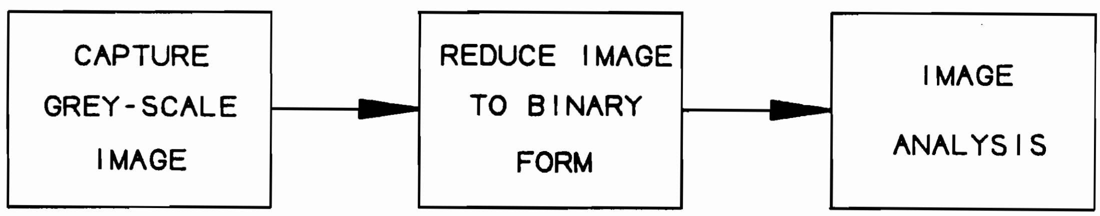

Figure 4.7 General optical scanning procedure

Many statistically-based algorithms for creating and analyzing binary images have been developed at Oregon State University by researchers such as Forrer (1987) and Funck _et_ _al_ (1987) for defect detection in veneer grading applications. These researchers have written and compiled a library of scanning subroutines in a software package called "VMENU" which can determine the precise locations of blob centroids in binary images. Surface displacements can be guaged in this manner and, thus, can enable strain values to be derived. With these prescribed algorithms and software available, the development of an optical scanning technique to measure surface strains was facilitated considerably.

4.3.2 Hardware and software development

The optical scanning system was comprised of a video camera, image capture board, microcomputer, and scanning software. A flowchart of the system is shown in Figure 4.8.

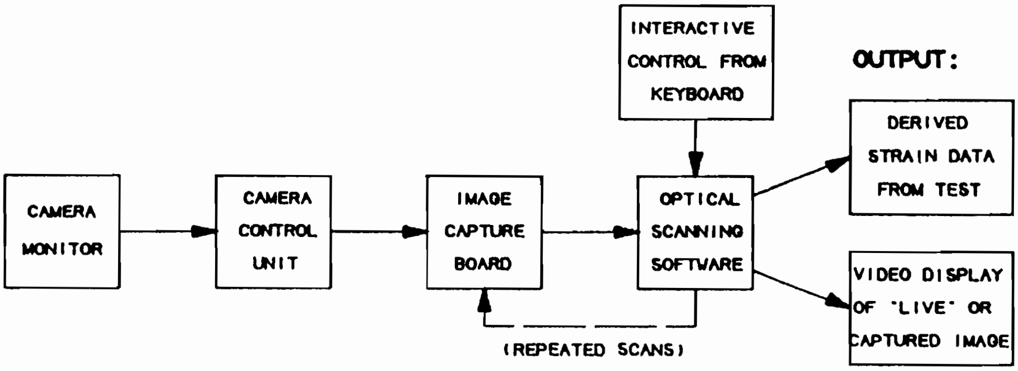

Figure 4.8 Schematic of optical scanning data acquisition system

4.3.2.1 Hardware:

A solid-state (Couple-charged), gray-scale, medium resolution video monitor (manufactured by Koyo - model YS-A10) was used as the optical pickup device. The CCD camera was selected in preference to a tube type camera; offering lower levels of image distortion and camera compactness. The camera resolution, which in this case was 510 X 492, indicates the number of picture elements (pixels) that are digitized when an image is scanned. Each grey-scale pixel can be described by its two characteristics of brightness and placement. The digitizer quantizes the original image and assigns brightness and coordinate values to each picture element. It is contained within a separate camera control unit, which also provides power to the camera's photosensitive surface and an analog signal to the image capture board (ATT model Targa 16) within the microcomputer.

The scanning process transfers information one line at a time to the capture board, with the video signal voltage corresponding to the brightness of each pixel. A synchronization pulse at the end of each line initiates the next line scan. Upon receiving the completely digitized image, it is stored in memory on the image capture board, where it is reduced to a binary image and analyzed with the scanning software. Many hardware functions such as the production of video monitor (live) images and scan initiation were triggered through the software.

4.3.2.2 Software

Subroutines employed:

As mentioned earlier, many subroutines in the VMENU software library were utilized in creating an operable program for optical scanning. The following list contains the subroutines, and their functions, which were linked together in the developed program:

MODE 512 - Clears storage space on the image capture board for 512 X 512 digitized resolution.

GRAY - Configures the image capture board to receive grey-scale images.

BLIVE - Creates a "live" image display from the camera on a monitor with a fixed border.

SETWINDOW - Initializes the use of a cursor to define a window size for capturing images.

SETBOTH - Allows both input and output window sizes to be the same.

GRAB IMAGE - Triggers the digitizer to capture the live image at that instant.

THRESH - A specific gray-scale threshold level is set which transforms the captured image to contain exclusively black and white picture elements. Pixels that are darker than the set gray-level are set to black, and those lighter, to white. This clarifies the edge definition of the black dots against the variable wood background.

CREATE BL - Creates a blank list of the expected number of dots to be searched for on the captured image.

CONNECTIVITY - Searches the scanned and thresholded image for the dots. This is accomplished using statistical algorithms pixel by pixel, determining if dark pixels are isolated or clustered. From the assembled information, the horizontal and vertical pixel coordinates are calculated for each dot.

BDISP - Displays information about the dots found in the captured image related to the connectivity analysis.

Calculating strain values:

A program was written in the programming language "C" to tie together this library of subroutines to accomplish the task of measuring strains on the surfaces of the thin wood beams as they deformed. A copy of this program can be found in Appendix A.

Ideally, the scanning system would have provided biaxial strains at selected locations. However, a system with such capabilities would have involved considerably more time to develop and evaluate. Instead, only uniaxial strains along the beam axis (horizontal) were measured, since principal strain trajectories are predominantly axial in flexed beams. Arrays of dot pairs were arranged along vertical cross-sections of the specimen. Displacements between dots in each pair relative to one another were monitored to enable strain values to be calculated.

Referencing strain magnitudes to their position within the selected vertical section of the beam yielded mappings of uniaxial (horizontal) strain.

Connectivity analysis concerns the detection of patterns among pixels with commonality, and here it enables blobs to be detected on a pixel-by-pixel basis using consistent sorting criteria. A connectivity analysis was carried out for each scan, after converting the image to binary form, to detect each dot pair and subsequently determine the precise separation of their centroids (see Figure 4.9). A comparison between image data collected before and after beam deformation provided a means for calculating displacements between the horizontally arranged dot pairs. By dividing these diplacements by the original dot positions prior to loading, numerical values of horizontal strain could be ascertained.

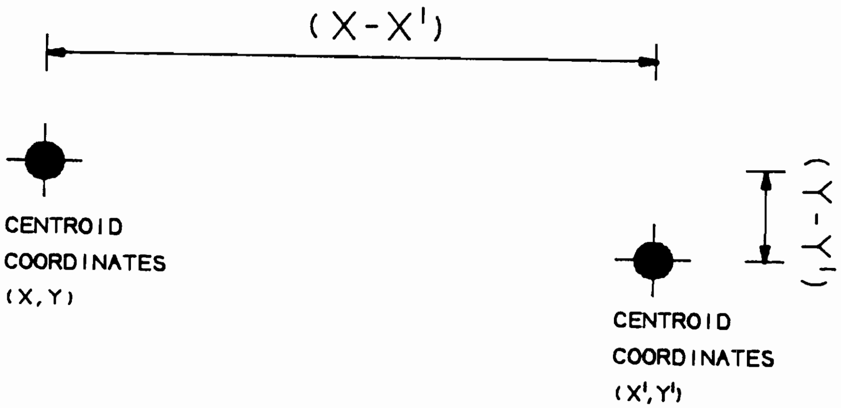

$$\text{DOT SEPARATION} = \sqrt{(X-X')^2 + (Y-Y')^2}$$

Figure 4.9 Method for geometrically calculating dot separations

Geometrical corrections:

To ensure proper calculation of the separation between paired dots, a test was performed to determine if there were any differences in the vertical and horizontal dimensions of the camera's pixels. This information was not available from the camera manufacturer, but was necessary for proper calulation of strains. For the test, a dot pair mounted on a rotating disc was placed in front of the video monitor. Progressive scans were made of the dot pair as it was rotated through 360 degrees, and the derived apparent pixel distances between the dot centroids were plotted against rotation angle (see figure 4.10). A correction factor of 0.91 relating horizontal and vertical coordinates was derived and used in the scanning software.

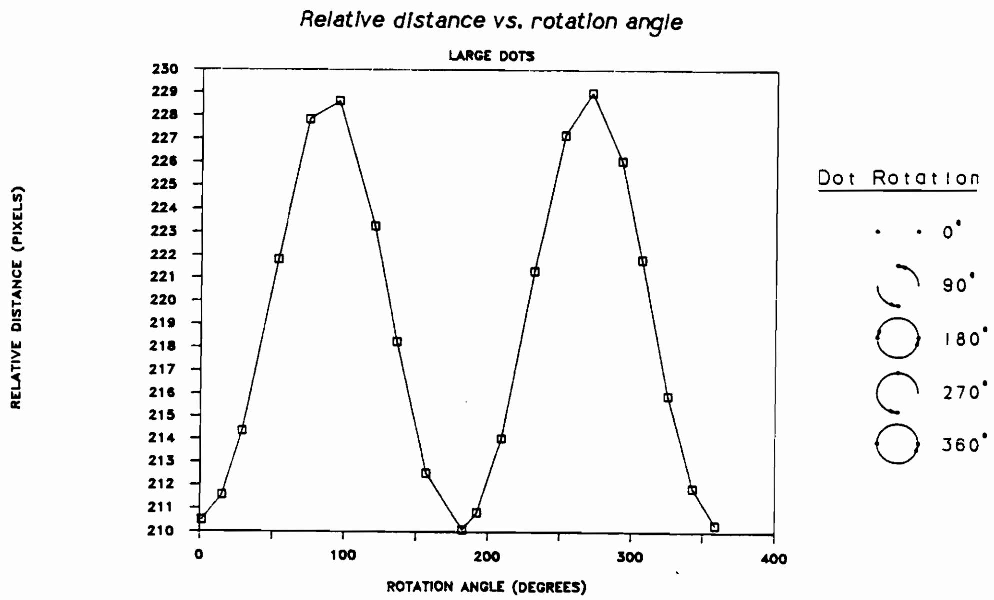

Figure 4.10 The effect of rectangular-shaped picture elements on the apparent separation of a dot pair when rotated through one revolution

Self calibration using reference dots:

Any slight changes in distance between the camera and specimen surface could result in distortion of the image and an incorrect measurement. Minute changes in lighting also influence the calculation of dot centroids and therefore may impair accuracy. To avoid these potential inaccuracies, a reference dot pair of similar size and separation to dot pairs fixed to the wood surface was also included in each scanned field. These reference dots were bonded to a small metal tablet which did not deform with the beam. Figure 4.11 describes the process by which strains were calculated with the aid of the reference dots.

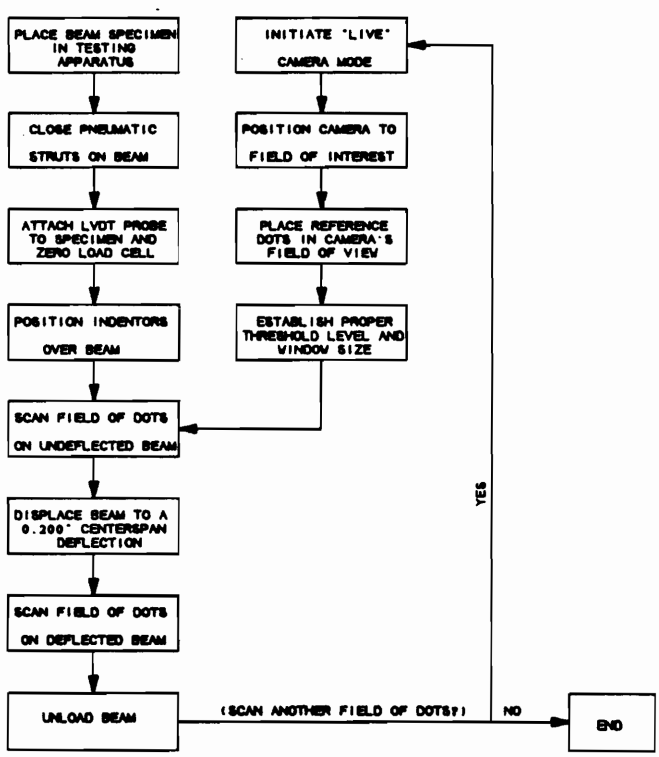

Figure 4.11 Flow chart describing the process for deriving strain data from scanned images

Implementation of the software:

The optical scanning program which was developed enabled the user to customize the scanning setup for a broad range of testing conditions. Connectivity analysis can only be performed on captured images which are in binary form. It has already been pointed out in section 4.3.1 that binary images were obtained by a thresholding process that converts a continuous grey-scale image to one with only two "colors", black and white, much like a silhouette. This was accomplished in the software by comparing the brightness of each pixel to a common assigned threshold (brightness level). Since the tonal appearance of wood is highly variable, the appropriate threshold setting was selected determined for each wood type on an individual basis. This allowed an optimal threshold setting to be chosen for each set of scans.

Prior to each series of scans, it was necessary to enter the number of dot pairs in the field and the position of the reference dots relative to those to be measured. A provision was made to automatically average multipally scanned fields to improve strain resolution. Scan delay time, the number of progressive scans, and scanning window size could also be chosen prior to execution.

4.3.3 Evaluation of the scanning system

The thresholding and connectivity features of the scanning software make exact replication of two seemingly similar images impossible. As a result, even a stationary object will appear to change position slightly with repeated scans. It is partly because of this instability that resolution is finite. The primary purpose in testing the scanning system was to determine how strain resolutions could be maximized, given the limitations imposed by the camera and image capture board. A number of variables were found to influence resolution. These were (1) field of view, (2) dot size, shape, and edge definition, and (3) averaging of multipally scanned fields. The effect that each one of these factors had on scanning precision was determined.

Field of view:

Camera field of view, the surface area on the specimen being monitored by the vision system, has little effect on proportional resolution. However, the paired dot separation within the field has considerable importance. Greater dot separations allow higher resolutions of strain within a given field. Therefore, zooming in on arrays of dot pairs until the dots lay just inside the viewing margins was desireable.

Dot size, shape, and edge definition:

Increases in dot size improved resolution significantly. Figure 4.12 illustrates how stability of the dot centroid from one set of scans to the next was enhanced with progressive enlargement of dot diameter. A disadvantage of using large dots is, however, that they can distort in shape and not displace precisely with the deforming fibers when the material is strained. A dot area of roughly 300 pixels was selected as a compromise.

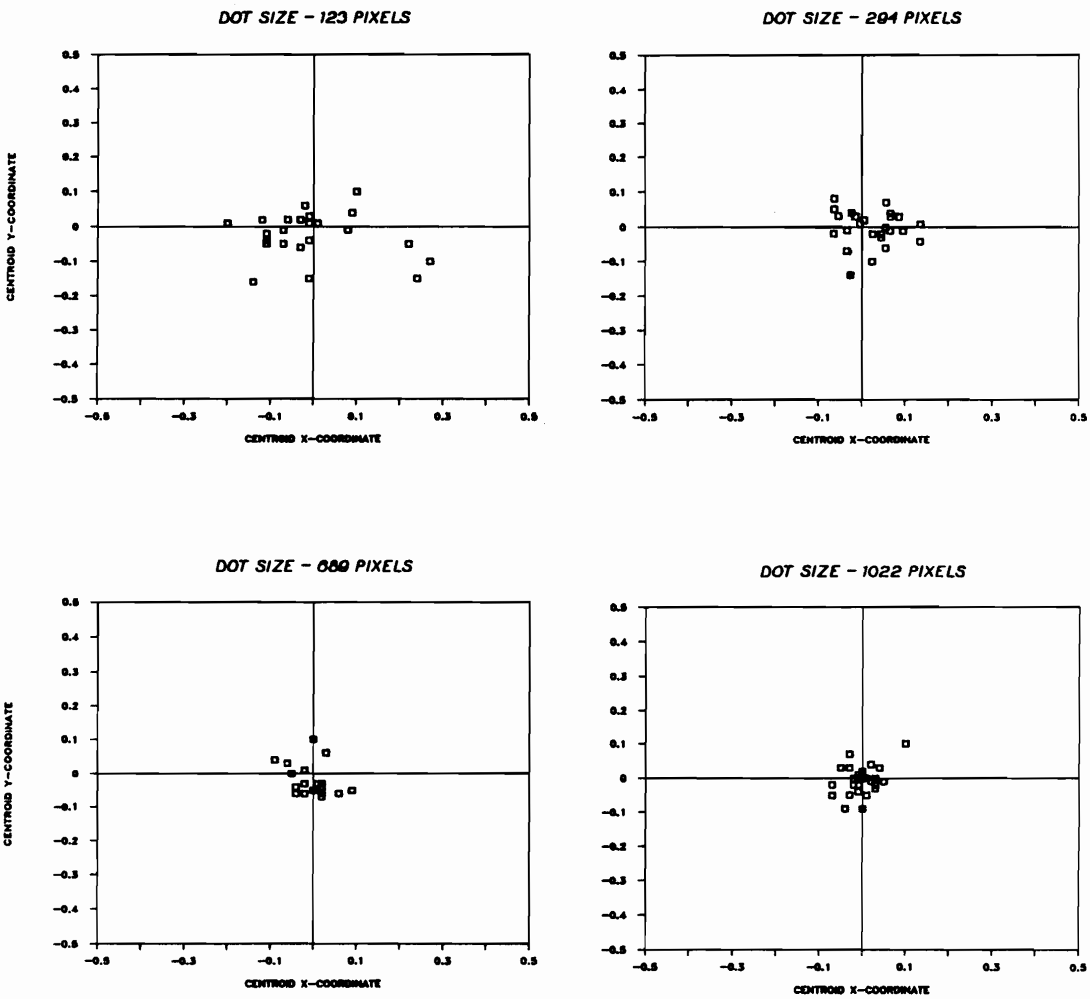

Figure 4.12 The influences of dot size on scanning variation. Plotted is the variation from the mean dot coordinates in pixels)

The shape of the dots also influenced scanning precision. The stability of round dots was found to be superior to that of square, triangular, or diamond shaped ones. Perhaps dot stability is related to its perimeter to area ratio. Intuitively, this seems reasonable because it is at the edges of dots that differences occur between scans (see below).

Poor definition along the edges of dots in a scanned image had a detrimental effect on resolution. Dot quality, lighting, background tone, and thresholding all controlled edge quality. Manufactured "rub-on" dots were superior to hand-inked dots for edge smoothness. Incandescent lighting produced undesirable shadows along the dot fringes and elevated the temperature of the specimen. A circular flourescent light, however, provided more uniform and cooler illumination. Sharp contrast between a black dot and the background tone produced excellent results. Measurement accuracy favored lighter colored woods, and separate calibrations on different woods were necessary. Excessive thresholding created an uneven dot perimeter, highlighting once again the advantage of using a light colored background material. All of these observations were useful for setting up optimal scanning conditions.

Averaging scans:

Multiple scanning and subsequent averaging of each field enhanced optical resolution considerably. Figure 4.13 shows the relationship between number of averaged multiple scans and resolution in terms of strain stability between pairs of dots. The benefits of averaging appeared to taper off at approximately ten scans.

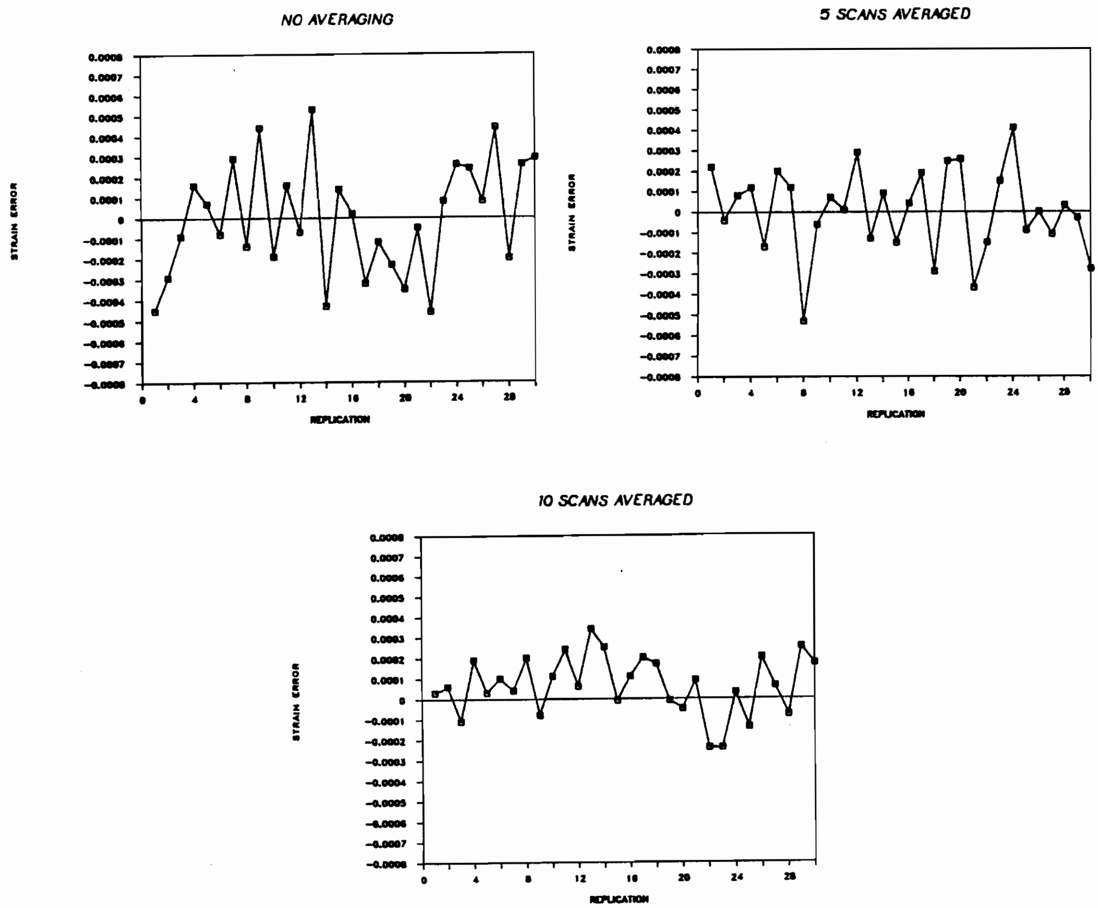

Figure 4.13 Demonstration how strain variability (system noise) is reduced by averaging multiple scans

4.3.4 Design of peripheral equipment

Camera tracking system:

A mechanism was designed to synchronize movement of the video monitor and the portion of the deflecting beam to be scanned. This enabled the camera to follow a particular field of dots on the specimen surface without any manual adjustment. The camera itself was held in a clamping device which was attached at the base to a universal mount. The camera mount was fastened to a counterweighted balance arm that pivoted at the center on a vertical post. A slide bar which cantilevered from the support base provided the necessary range adjustment for the camera. The camera could be repositioned along the length of the specimen by loosening machine screws where the slide bar connected to the support base. A light tracking arm extended from the camera mounting to the underside of the beam. This allowed the camera to follow the beam movement as it deflected. The entire camera mounting/tracking device shown in Figure 4.14 was constructed of lightweight aluminum so as not to induce significant torsion on the support base.

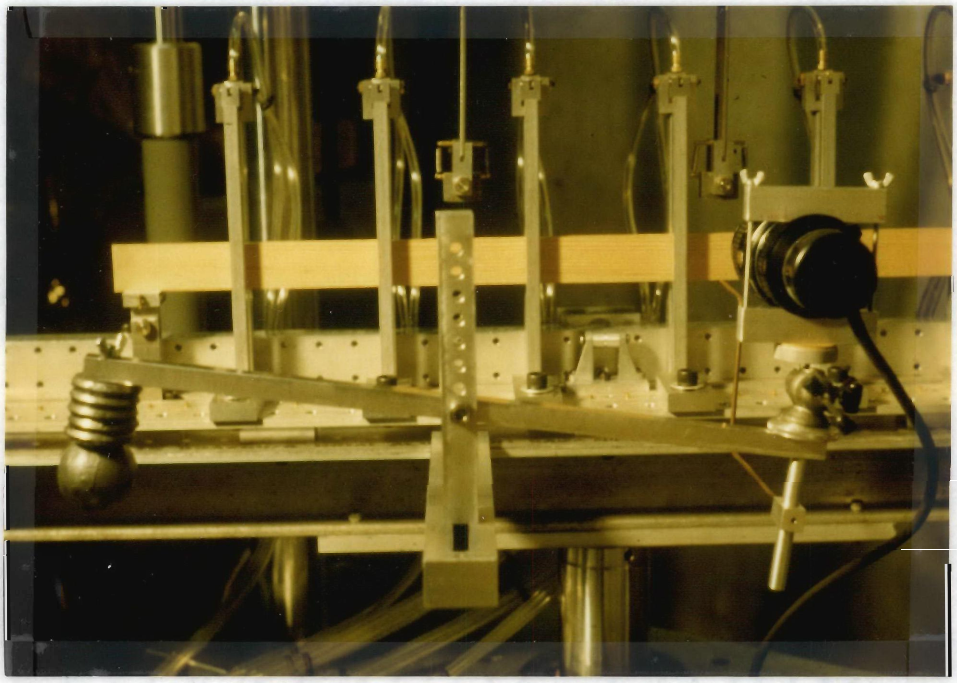

Figure 4.14 Photograph of camera mounting/tracking device

Reference dot tab:

The reference dots were fixed to a small piece of sheet steel (0.5" x 0.125" x .025") which was colored white to minimize reflective glare. A magnetic strip hanging on the backside of the beam held the metal reference dot tablet to the specimen surface. A notable advantage to this method was that adhesives were not needed to hold the reference dot tablet in place.

4.4 Specimen Preparation

4.4.1 Selecting appropriate test materials

Although of secondary importance to technique development, the selection of appropriate test materials was a significant aspect of this study. In Chapter 2 was the need for continued research on the behavior of both dimension lumber and laminated beams was addressed. Both are important structural materials, but dimension lumber was not included here due to time constraints. The decision favoring laminated beams was based upon the premise that the properties of composite materials, being more controlable, could enable a clearer demonstration of the technique's attributes. However, applicability of the technique is general, and is not limited to laminated beams.

Two important features in laminated beam construction effecting mechanical properties are laminae stiffnesses and the location of knots within the beam's section. To simplify the study of these two factors, specimens were designed to examine these characteristics separately.

Therefore, specimens used in the study of elastic effects were constructed of clear laminae, while knot influences were investigated with laminae of comparable elastic moduli.

Beams commercially manufactured in the Northwestern United States utilize a broad variety of wood species. Of these, Douglas-fir (Pseudotsuga menziesii) and Western White Pine (Pinus monticola) were selected for the study. Douglas-fir harvested from various geographic regions and stand ages can vary widely in specific gravity, and this influences elastic properties. This species was therefore used to evaluate strain interactions between laminations due to combinations of laminae with contg stiffnesses.

Abrupt demarcations between stemwood and knotwood, a common characteristic of Western White Pine, leads to highly localized grain deviations in the knot's vicinity. This feature enables one to better establish true margins of the knot, which makes this species well-suited for this second aspect of study.

Differences in surface coloration of these two wood species were expected to yield dissimilar strain resolutions. Both wood types were assessed for attainable scanning resolution and the derived data enabled data truncation criteria to be formulated. Resolution was determined by scanning thirty fields (averaging ten images for each field) of a static array of dots on the two wood surfaces. The largest deviation from zero strain was interpreted as indicating maximum error due to system noise. Plots from these tests on both wood species are shown in Figure 4.15. It appeared that strain resolution on a typical Douglas-fir specimen was 500 microstrains, whereas a 400 microstrain precision could be obtained on the Western White Pine.

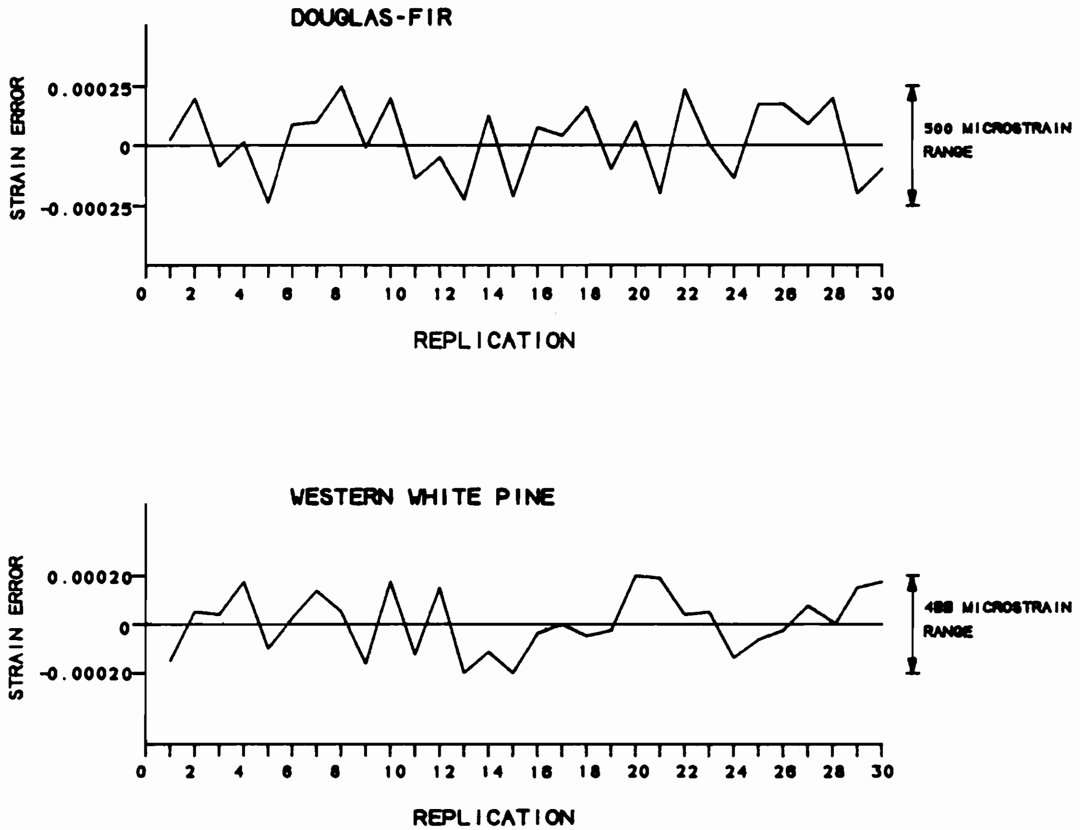

Figure 4.15 Strain error (system noise) observed on Douglas-fir and Western White Pine specimens

The above concerns resolution of stationary dot positions. Resolution of incremental displacement is another aspect of system performance. This was investigated by mounting dots on a moving stage which could be positioned with an accuracy of 0.0001". Strain data, using optical scanning, was collected five times at each measured displacement for both wood species. This data (Figures 4.16 and 4.17) suggests that noise inherent in both static and displaced images is limiting. The vertical component of the "bandwidth" of the plot reflects the precision of the scanning system for sensing strains.

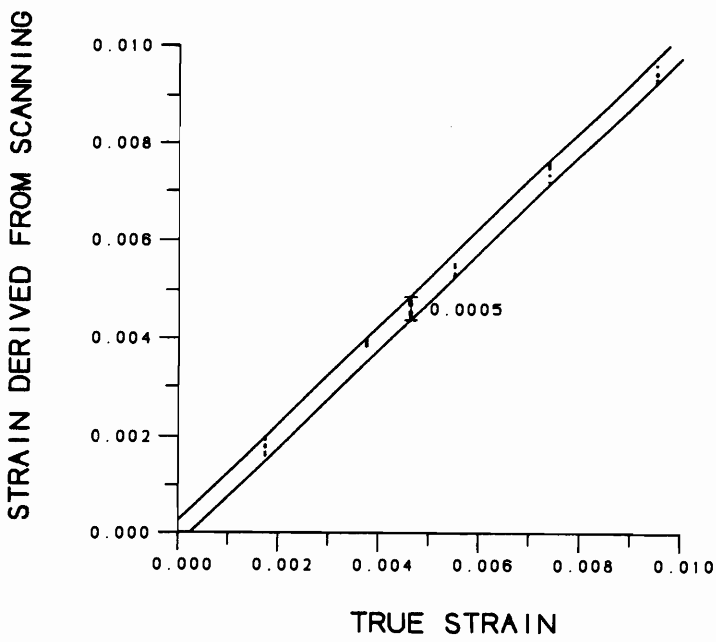

Figure 4.16 Scatter plot of apparent strain (from optical scanning) versus measured strain using a calibration device (Douglas-fir)

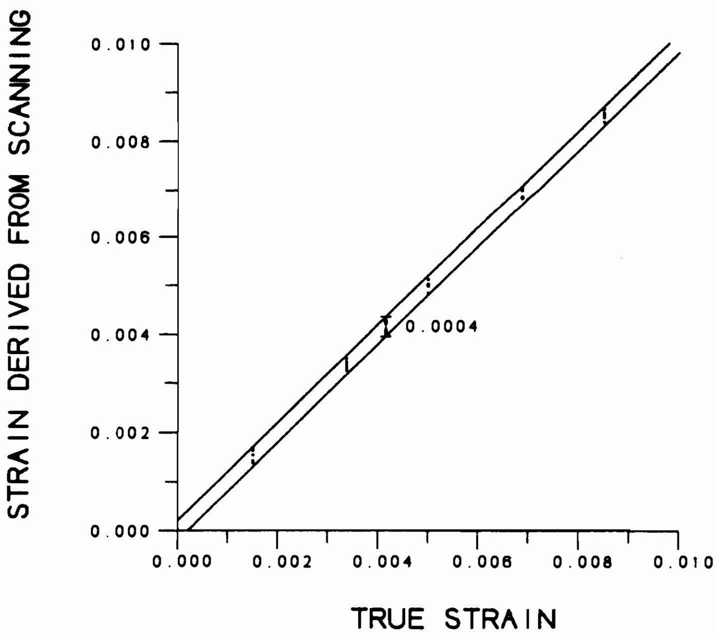

Figure 4.17 Scatter plot of apparent strain from optical scanning versus measured strain using a calibration device (Western White Pine)

4.4.2 Preparation of laminating stock for test beams

Flat-sawn boards of Douglas-fir, relatively free from defects and having contrasting specific gravities (0.47 and 0.40 respectively) were selected, as well as Western White Pine (WWP) with round knot defects, as stock material from which the specimens were fabricated. The stock boards were planed on the tangential face to a thickness of 5/8". Strips 3/8" wide by 40" in length were radially sawn from these surfaced boards, labeled, and then brought to a 12% equilibrium moisture content during a two week period in a conditioning room. With the exception of WWP strips containing knots, the prepared specimens were loaded nondestructively to determine Moduli of Elasticity. This tabulated data on each wood strip was then used as the criteria for the selection of pieces incorporated within the laminated beams.

4.4.3 Lamination configurations

The effects of stiffness and the presence of knot defects within constituent laminae of complete beams were evaluated by manufacturing and subsequently testing a range of beam designs. The beams listed in Tables 4.1 and 4.2 were fabricated, using a phenol resourcinol adhesive, to provide a broad assortment of beam types for evaluation. A non-laminated, clear Douglas-fir beam recorded in Table 4.1 was also included for comparitive purposes. In the WWP beams listed in Table 4.2, the knot defect was located in the center of the span of the associated lamination. The knot was encased, vertical, and approximately 3/4" in diameter. After allowing adequate curing time, the beams were planed to a .250" (+- .010") thickness and trimmed to a 2.50" depth and 38" length (36" span).

LAMINATION POSITION WITHIN BEAM	BEAM 1	BEAM 2	BEAM 3		BEAM 4		BEAM 5	
			CONFIG 1	CONFIG 2	CONFIG 1	CONFIG 2	CONFIG 1	CONFIG 2
TOP	2.01	2.67	1.26	2.86	3.37	3.08	3.05	1.08
UPPER MIDDLE		1.40	1.38	2.80	1.64	3.30	1.19	3.00
LOWER MIDDLE		1.41	2.80	1.38	3.30	1.64	3.00	1.19
BOTTOM		2.63	2.86	1.26	3.08	3.37	1.08	3.05

Table 4.1 Arrangement of laminations for Douglas-fir beams according to Moduli of Elasticity (units = x 10 psi)

LAMINATION POSITION WITHIN BEAM	BEAM 1		BEAM 2	
	CONFIG 1	CONFIG 2	CONFIG 1	CONFIG 2
TOP	KNOT	2.26	2.47	2.32
UPPER MIDDLE	2.52	2.37	2.27	KNOT
LOWER MIDDLE	2.37	2.52	KNOT	2.27
BOTTOM	2.26	KNOT	2.32	2.47

Table 4.2 Arrangement of laminations for Western White Pine beams, one lamination which contained a knot defect. Moduli of Elasticity are shown in units x 10 psi.

4.4.4 Beam surface preparation

Hand sanding the beam surfaces with fine grained sandpaper was necessary to assure proper adhesion of the arrays of dot pairs to the wood surface. This also minimized shadowing from surface irregularities. Sets of dot pairs, each separated in the horizontal plane, were arranged vertically on the surface of all Douglas-fir beams at the center of the span. The WWP beams had two arrays of dot pairs. One array contained the knot within its vertical section. Unfortunately, the dark color of the knot prevented strain measurement within the knot itself. The other was positioned 1" away, adjacent to the knot. This enabled the influence of the knot on strain distributions within its vertical and horizontal vicinity to be evaluated. Horizontal separation between the .005 inch diameter rub-on dots on all specimens was approximately 1/2". Accurate and consistent dot separations were not crucial since strain values are derived from relative movements. Vertical spacing between each dot pair was about 1/10", which allowed for nearly twenty-five pairs in each vertical beam section. The prevalent dark gluelines were hidden in the vicinity of the dots using "White-Out" to improve background contrast.

4.5 The testing method

4.5.1 The testing setup

Since this research work was principally concerned with elastic deformations, the test beams were loaded non-destructively to moderately low levels of strain. Also, in order that high resolution strain data could be obtained for localized areas, it was necessary to restrict measurement to small portions of the beam at one time. As a result, each beam was loaded and unloaded several times to enable strain information for complete cross sections to be accumulated. Repeatability of flexural behavior under cycled loading could be reasonably assured by limiting deflections to 50% of the anticipated proportional limit. This approximate value was experimentally determined from a load versus midspan deflection curve obtained from a comparable Douglas-fir test beam (H=2.5", B=1", L=36") which was loaded to failure. The deflection limit was determined to be 0.200" at midspan. The MTS servohydraulic testing machine was programmed in the strain control mode to provide a relatively rapid beam loading and unloading rate of two inches per minute, peaking at this midspan deflection. Figure 4.18 displays the beam loading cycle which was triggered and disabled manually. Maximum deflection was maintained for approximately 60 seconds, which enabled ten scans to be taken of the strained beam.

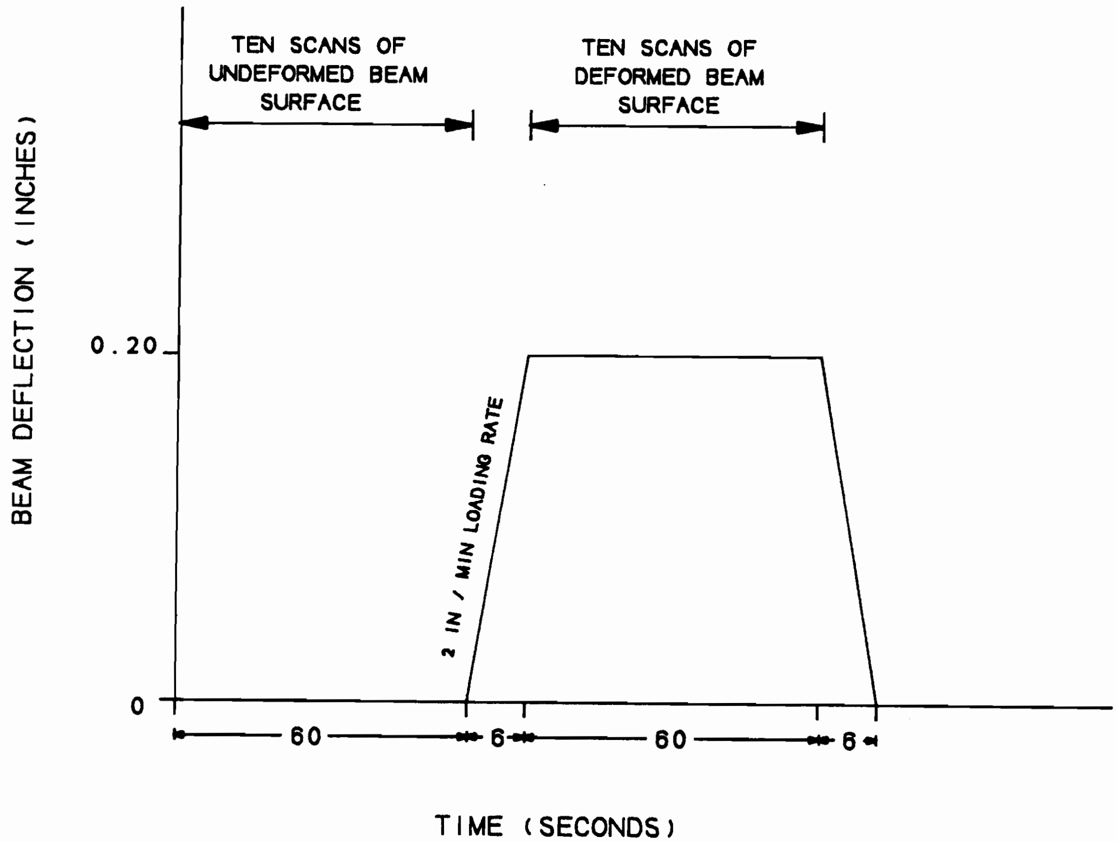

Figure 4.18 Load cycle used for testing all beam types

The load versus midspan deflection curve, used to establish a 50% proportional limit deflection, also provided useful information to calculate the appropriate placement of the struts to maintain lateral stability of the beams during the test. The following stability equation (Chajes, 1974) was used to determine the adequate strut spacing along the beam length:

$$L = \left(\frac{S_x}{M}\right)(b)(\pi\sqrt{GE})\left(\sqrt{\frac{I_Y}{I_x}}\right) \qquad (4.1)$$

WHERE:

- L = REQUIRED LATERAL SUPPORT SPAN
- b = BENDING MEMBER WIDTH
- M = BENDING MOMENT
- S_x = SECTION MODULUS ABOUT X-X AXIS
- I_x = MOMENT OF INERTIA ABOUT X-X AXIS
- I_Y = MOMENT OF INERTIA ABOUT Y-Y AXIS
- G = MODULUS OF RIGIDITY
- E = YOUNG'S MODULUS

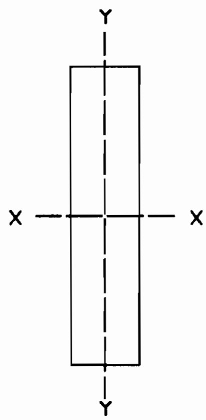

The bending moment variable (M) within the equation was derived from the forementioned Douglas-fir test beam data, also taking into account differences in width and size factor (Chapter 3). The constants E and G were assigned the tabulated values for West coast Douglas-fir ($E = E_L$ = 2.14 x 10 psi, $G = G_{RT}$ = 1.234 x 10 psi) published by Bodig and Jayne (1982). Lateral support spans were assumed to be the same for WWP beams because of offsetting effects of E and G with bending moment at the specified deflection. An unsupported length of 6.12" was calculated for the beam at the predicted maximum moment. Conservatively, the struts were placed at 6" intervals along the length of the beams.

Strut restraining pressure was held constant for all beam types through the air regulator at 20 psi. This pressure translated to a piston thrusting force of 2.5# against the beam face at each strut location. Frictional resistance to beam displacement at this pressure was negligible.

Although of secondary importance, a load versus midspan deflection curve for each beam was recorded on an X-Y recorder from signal outputs from a load cell (above indentors) and a linear variable differential transformer (LVDT) positioned below the beam. This information was necessary for discerning relationships between elastic microstrain distributions and complete beam behavior.

A bracket extending from the MTS frame held a fluorescent light which encircled the video monitor lens and illuminated the specimen surface. The video monitor was mounted with its optical axis perpendicular to the beam face. The camera control unit and computer data acquisition system were located next to the MTS machine to facilitate coordination of mechanical beam loading and scanning. Figure 4.19 shows the testing apparatus in its entirety.

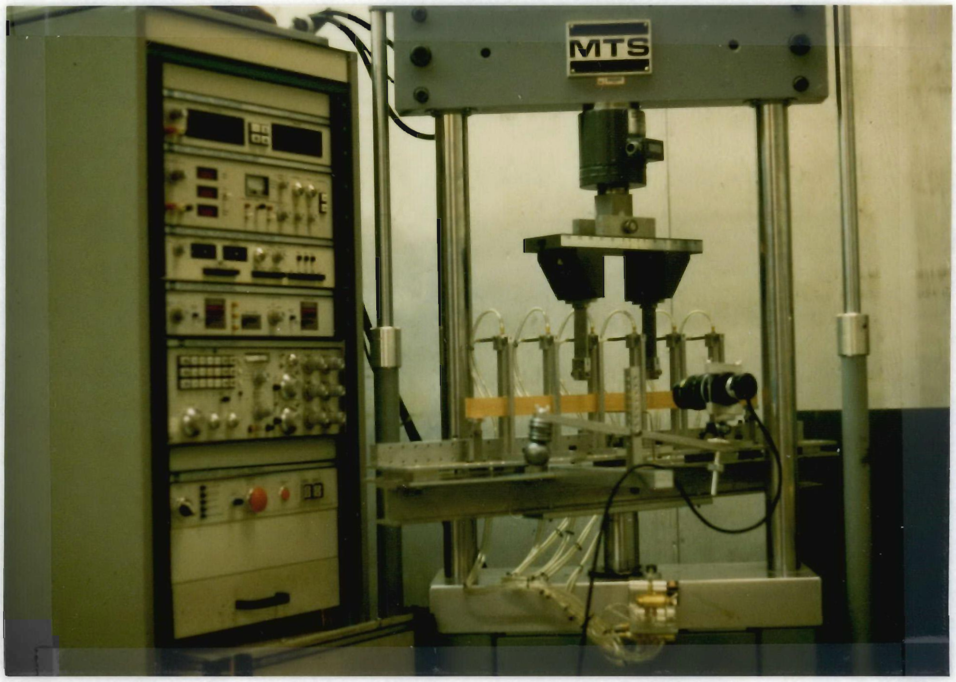

Figure 4.19 The complete testing assembly

4.5.2 The testing sequence

Figure 4.20 shows how strain information for an entire beam cross-section was accumulated from a series scans made at different vertical positions under similar deflections. Evaluation of each field involved sequentially comparing dot separations in the unloaded and loaded (0.200" deflection) conditions; data from ten scans were averaged for each. The reference dots were moved from field to field to enable implicit correction of every field to be achieved. Unfortunately, the width of the reference dot tab required covering at least one pair of the narrowly spaced dots on the beam surface. However, by overlapping fields, strain values could be obtained for the entire beam's cross-section. Figure 4.21 provides a general flow diagram of the entire testing sequence.

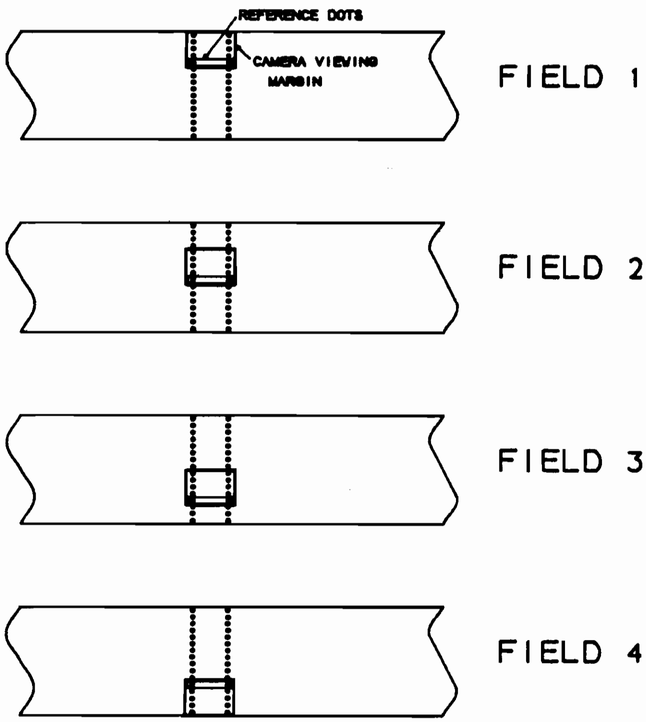

Figure 4.20 Method for accumulating strain data for a complete beam cross-section by compiling data from smaller fields

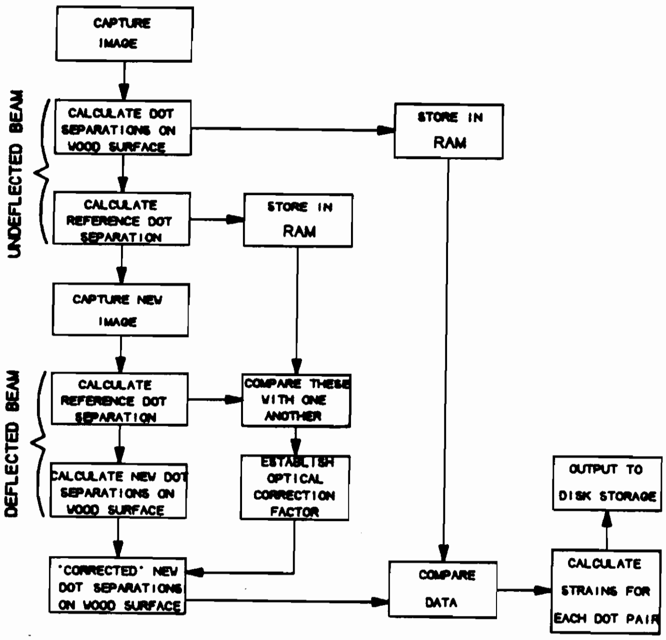

Figure 4.21 Summary flow chart of the testing process

4.5.3 Data collection and reduction

Data obtained from scanning each beam was saved on two individual files in ASCII code. One file included a record of the apparent changes in separation between the reference dots from one scan to the next. Although this information was not used in data analysis, it helped in the detection of system malfunctions which may have lead to errors in the derived strain output. A second file contained sets of strain values themselves relative to their positions in the beam. For proper assembly of this data file, the fields scanned on the beam proceeded from the top to the bottom of the beam. These data files were subsequently transfered to a LOTUS spreadsheet for analysis. The precise location of each recorded strain, derived from a specific dot pair on the beam surface, was measured with digital hand calipers and entered on the spreadsheet adjacent to its corresponding strain value. In this way, mappings of strain relative to position in the beam section could be plotted.

Load versus centerspan deflection plots obtained during the tests from the X-Y recorder were used to derive composite MOE values for the beam material. The following formula was used (ASTM, 1986f):

$$MOE = \frac{P\,L^3}{C\,b\,h^3\,\Delta} \qquad (4.2)$$

where:
P = applied load
L = beam span
b = beam width
h = beam depth
Δ = beam deflection at load P
C = 4.7 = loading configuration constant

It should be remembered that the values so derived make no account for the variations in material properties throughout the beam and are predominantly influenced by the extreme fibers.

4.5.4 Data presentation format

Derived strain values were truncated in accordance with the resolution of the system. This process generated "stair-stepped" scatter plots of the data relative to position within the beam. These plots clearly do not imply abrupt transitions of strain in the material but merely reflect the usage of the rounded values. An approximation of the actual strain distribution was made by fitting a smooth curve through the mean position of each strain level in the beam. Tensile strains were represented as positive values and compressive strains in the negative sense. These plots of strain are discussed in Chapter 5.

CHAPTER 5

RESULTS AND DISCUSSION

5.1 Introduction

This research centered on developing a technique which minimizes in-plane material variation such that the structure of wood-based specimens can be related directly to observed mechanical behavior. Such knowledge is necessary for the improvement of current theories of wood mechanics. It follows, therefore, that a convenient approach to evaluating the derived data would be to compare it with predictions using current theory. It should be emphasized, however, that the major concern of the thesis is the development of the approach as a tool for future use. The analysis and interpretation of results will, therefore, only be preliminary in nature.

The effects of both lamination stiffness and the inclusion of knots were studied separately for the range of beam types listed in Chapter 4. The beams were evaluated quantitatively by plotting each measured vertical strain distribution along with a corresponding curve derived using current elastic theory. Theoretical prediction of strain distributions becomes more difficult when the beams include knots and other discontinuities. However, by making a limiting assumption that a knot will only influence behavior within its own cross-section (non-contributing), plots of theoretical strain distributions could be calculated for these beams as well.

5.2 Establishing theoretical beam behavior

Estimates of strain levels at various positions within each of the various beam types can be calculated using a step-wise process outlined by Bodig and Jayne (1982). An assumption is made that elasticity is homogeneous for each lamination. The first step involves a transformation of each layer's width relative to a specified reference lamination, and this process yields an artificially transformed beam cross-section. It was assumed that the modulus of elasticity in tension is the same as that for compression and that deformations are linear within the elastic range of the material. The equation for transformation takes the form:

$$W_i = W\ (E_L^{\,i} / E_L^{\,n}) \qquad (5.1)$$

where:

W_i = transformed width of layer i
W = untransformed width
$E_L^{\,i}$ = longitudinal elasticity of layer i
$E_L^{\,n}$ = longitudinal elasticity of reference layer

The position of the neutral axis may then be calculated as follows:

$$\bar{y} = \sum_{i=1}^{n} A^i d^i \Big/ \sum_{i=1}^{n} A^i \qquad (5.2)$$

where:

$\bar{y}$ = location of horizontal centroid w/ respect to a reference plane
A^i = transformed area of layer i
d^i = transfer distance for layer i to reference plane

Moment of inertia may then be calculated using the "parallel axis theorem":

$$I^t = \sum_{i=1}^{n} (I^i + A^i(\bar{d}^i)^2) \qquad (5.3)$$

where:

$\bar{d}^i$ = transfer distance for layer i
I^t = moment of inertia of transformed body
I^i = moment of inertia of layer i

The normal strain distribution through the beam may then be calculated at any location after substitution of appropriate values for $\bar{d}^i$, w^i, and $E_L{}^i$ into the following equation:

$$\gamma_x = ((M\bar{d}^i \,/\, I^t)\ (W_i \,/\, W)) \,/\, E_L{}^i \qquad (5.4)$$

where:

γ_x = normal strain magnitude in horizontal plane
M = applied bending moment

The applied bending moment values required in this equation have already been experimentally obtained from load versus deformation curves for each laminated beam. Since linear elasticity is assumed for the transformed beam, strain magnitude should vary linearly with position within the beam cross section. These estimated deformation data were then combined with the experimentally obtained mappings for graphical comparison. On beams containing knots, an elasticity of zero is assumed within the cross-section containing the knot.

5.3 The behavior of beams with laminae of differing elasticity

Five different types of laminated beams were evaluated using the developed experimental technique. Each of these will briefly be considered in turn before going on to discuss general implications of the effect of constituent elastic modulae on beam behavior.

Beam type one (non-laminated, clear Douglas-fir):

Figure 5.1 displays the measured strain distribution within this beam when flexed, together with a theoretical line. Simple beam theory assumes that the neutral axis lies at the midpoint of the beam's vertical cross-section, as the predicted line shows. However, an upward shift of the neutral axis was observed, along with an associated higher level of strain in the tension (lower) zone. This clearly suggests that the material had differing compressive and tensile elasticities. At least one, if not a combination, of the following could explain this type of behavior:

(1) The sawn geometry of the member resulted in an uneven distribution of earlywood and latewood.

(2) Inhomogeneities or microfractures in the tension side of the beam caused localized weakening and reduced stiffness.

(3) Actual differences between compressive and tensile elasticities exist.

Careful examination of the specimen revealed a localized grain deviation of approximately eight degrees in the lower section of the beam extending to the edge. Calculations estimate that a 10% reduction in longitudinal stiffness may be expected from such a grain angle.

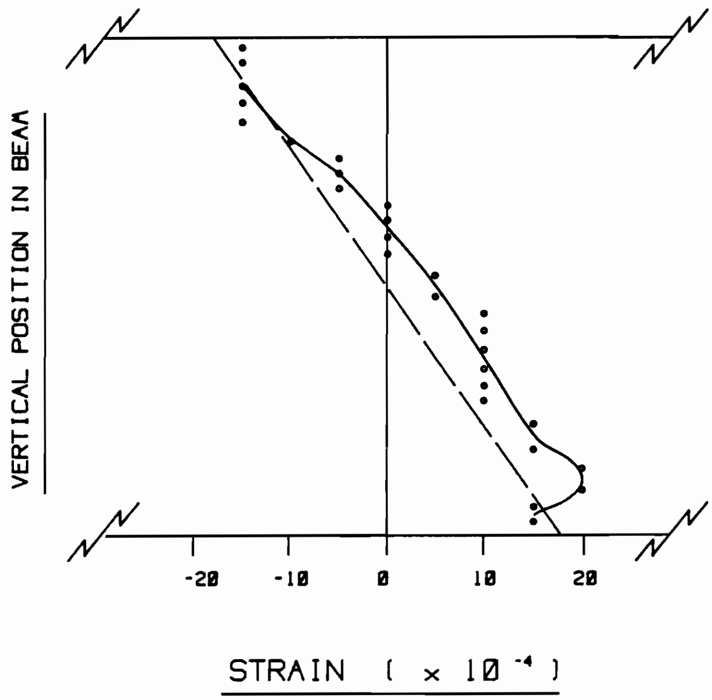

Figure 5.1 Mapping of measured strains at a 0.200" midspan deflection for the clear, non-laminated Douglas-fir bending specimen. The dashed line indicates theoretical distribution. (MOE = 2.01×10^6 psi)

The markedly higher level of strain observed in the fibers near the lower (tension) extremity of the beam may suggest that viscoelastic yielding began to occur at this location (despite the precautions taken not to exceed the "recoverable elastic" limit of the material). Also visible was a reduced strain in the immediate vicinity of the lower extreme fibers. This phenomena may indicate either a change in principal strain tradjectory or a local interruption in fiber continuity. In either case, it is likely that the altered grain angle in this region contributed to this behavior.

Beam type two (high outer laminae modulae and low inner modulae):

The distribution of modulae within this beam, together with measured and calculated cross-sectional strain distributions is shown in Figure 5.2. Clearly, measured values deviated significantly from predicted ones. The pronounced deviations in longitudinal strain levels in the two outer laminations may indicate preferential stress concentrations in those areas. The more flexible inner laminations did not appear to contribute much to the rigidity of the composite beam as evidenced by a large strain gradient within this section.

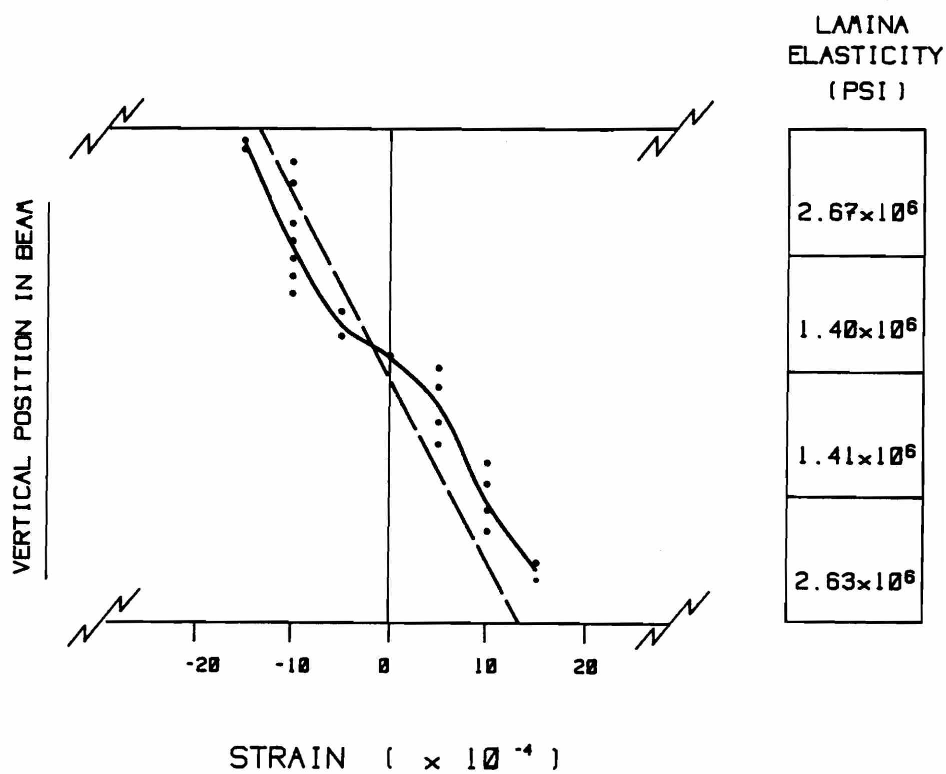

Figure 5.2 Mapping of measured strains at a 0.200" midspan deflection for the laminated Douglas-fir "beam 2". The dashed line indicates theoretical distribution. (MOE = 1.84 x 10^6 psi)

Beam type three (two high modulae laminae adjacent to two low modulae laminae):

This beam was deflected both with the high modulae material at the bottom (tension zone) and at the top (compression zone) and two sets of data were collected. These are shown in Figures 5.3 and 5.4 respectively. As would be expected, marked differences in mapped strains were observed between the two beam orientations. If the assumption is made that the material has equal elasticities in tension and compression, then one would expect experimentally-derived mappings for the two beam orientations to be mirror images of one another. However, when the more rigid laminae were uppermost (Figure 5.4), the neutral axis shifted dramatically due to increased deformations in tension. This shift did not appreciably effect the overall measured beam stiffness, but could significantly influence its total load carrying capacity.

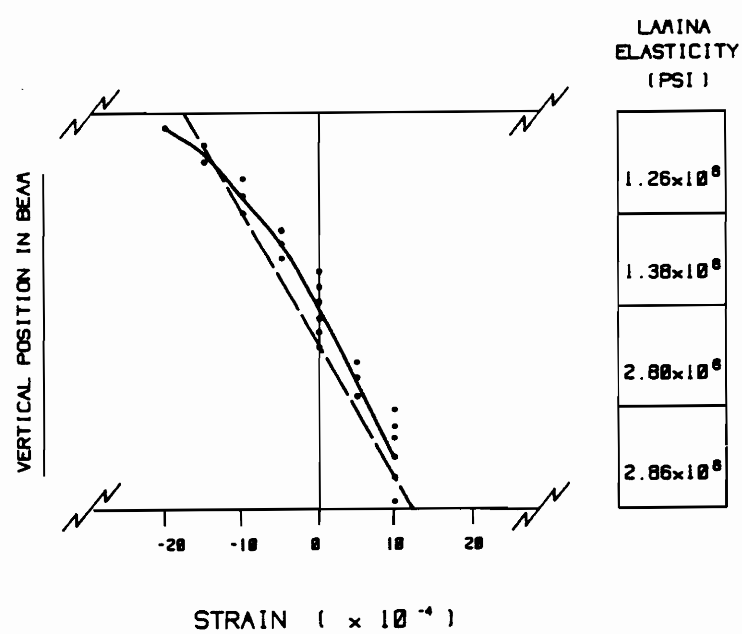

Figure 5.3 Mapping of measured strains at a 0.200" midspan deflection for the laminated Douglas-fir beam "3" with the lower modulus material uppermost. The dashed line indicates theoretical distribution (MOE = 1.46 x 10^6 psi)

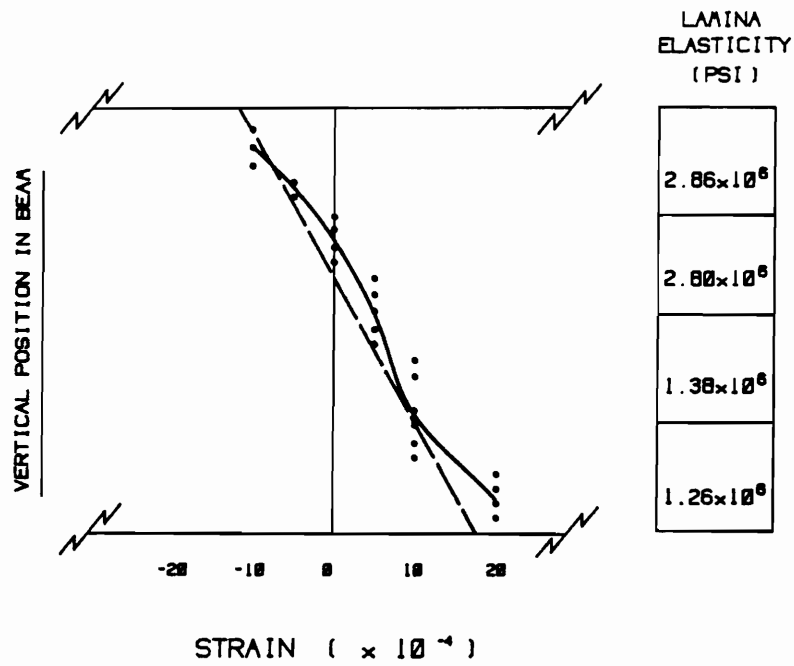

Figure 5.4 Mapping of measured strains at a 0.200" midspan deflection for the laminated Douglas-fir beam "3" with the higher modulus material uppermost. The dashed line indicates theoretical distribution. (MOE = 1.44 x 10^6 psi)

Beam type four (the inclusion of one abnormally flexible internal lamination):

This asymmetrical beam was also deflected in both its possible orientations and the derived mappings are shown as Figures 5.5 and 5.6. Figure 5.5 (with flexible lamination above the neutral axis) exhibits a rapid change in strain at the interface between the two center plies. This effect may also be seen in Figure 5.2 in which a similar situation prevailed. The feature is, however, curiously absent in Figure 5.6. Instead, strains are more highly concentrated in the outer tension flange. The effect of the presence of the flexible lamination clearly depends upon its location within the beam's section and how each lamination is stressed (tension or compression). Again, no significant change in complete member stiffness could be detected for the two orientations.

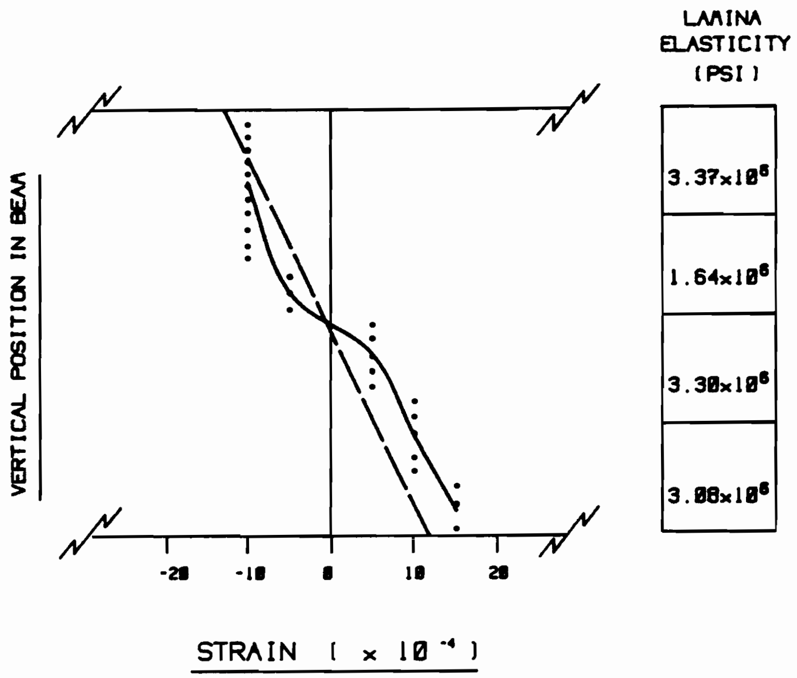

Figure 5.5 Mapping of measured strains at a 0.200" midspan deflection for the laminated Douglas-fir beam "4" with the flexible lamination lying above the beam center. The dashed line indicates theoretical distribution (MOE = 1.95 x 10^6 psi)

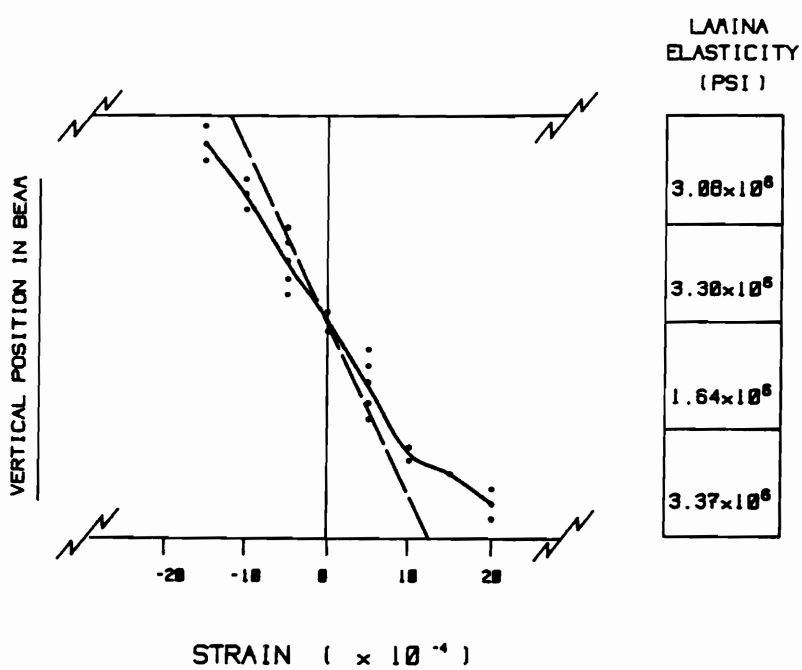

Figure 5.6 Mapping of measured strains at a 0.200" midspan deflection for the laminated Douglas-fir beam "4" with the flexible lamination lying below the beam center. The dashed line indicates theoretical distribution (MOE = 2.06 x 10^6 psi)

Beam type five (laminations of alternating high and low stiffness):

Distributions of strain are shown for this final beam flexed in its two possible configurations in Figures 5.7 and 5.8. A reasonably linear plot can be seen in Figure 5.7, which contrasts somewhat with Figure 5.8 which displays a rather more complex form. An explanation for inconsistencies between these two strain patterns may relate, once again, to differing tensile and compressive elastic behaviors of the laminations or preferential stress concentrations.

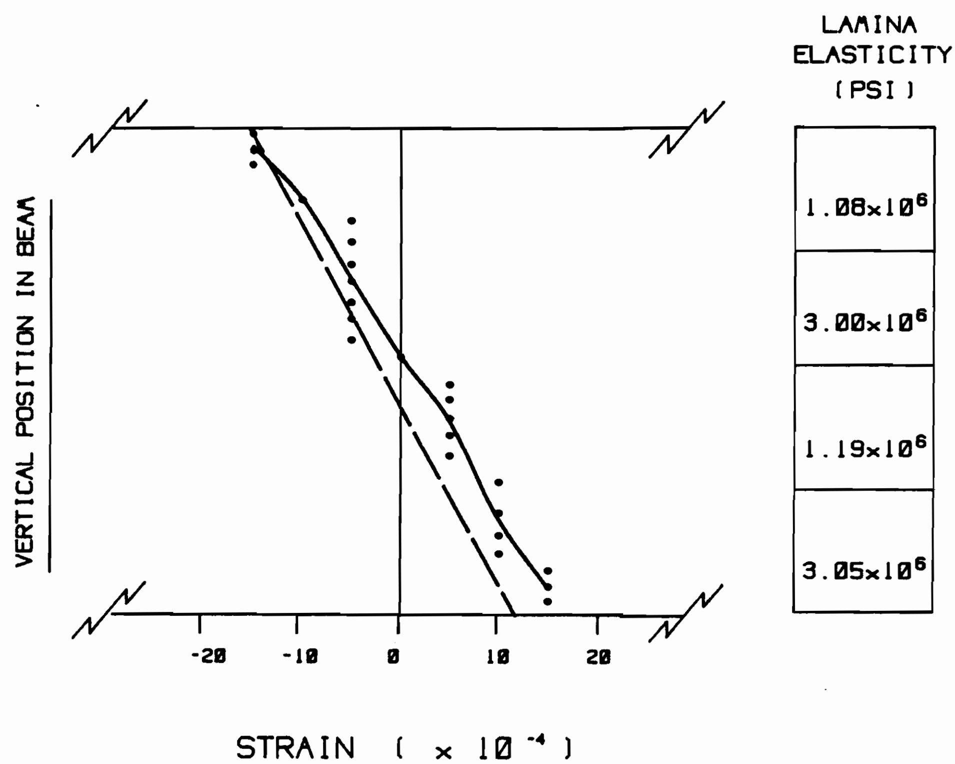

Figure 5.7 Mapping of measured strains at a 0.200" midspan deflection for the laminated Douglas-fir beam "5" with a flexible lamination uppermost. The dashed line indicates theoretical distribution (MOE = 1.36 x 10^6 psi)

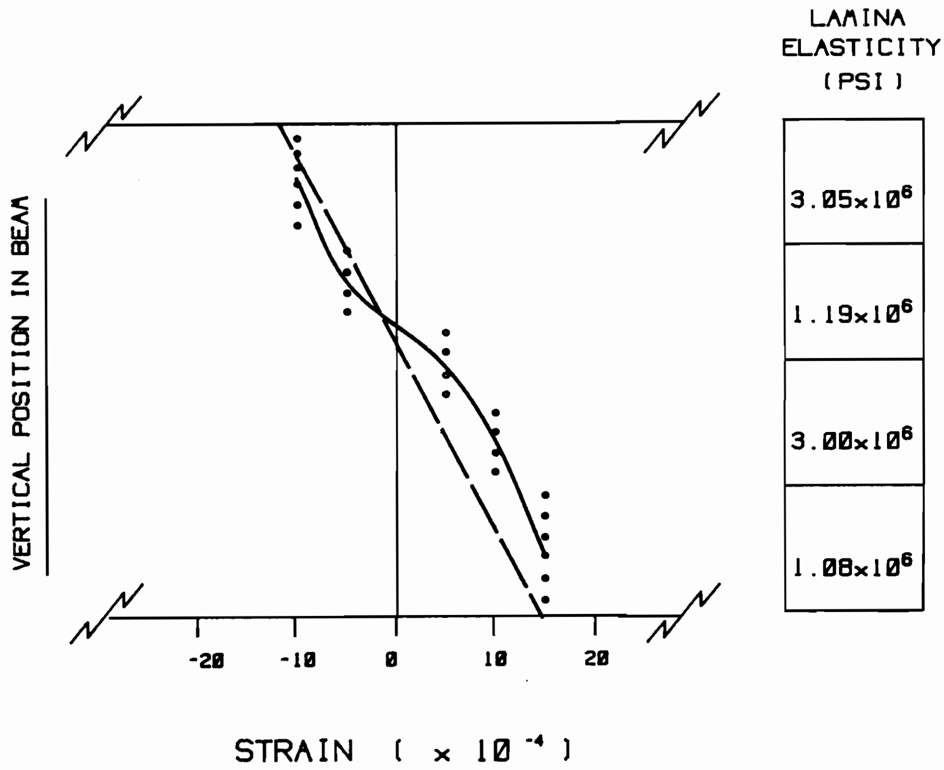

Figure 5.8 Mapping of measured strains at a 0.200" midspan deflection for the laminated Douglas-fir beam "5" with a rigid lamination uppermost. The dashed line indicates theoretical distribution (MOE = 1.38 x 10^6 psi)

Concluding observations for tests on beams with differing elasticities:

The experimentally derived strain mappings for the various beam types and orientations tested had several common features. Measured distributions were unexpectedly tortuous, which may indicate that deformations concentrate preferentially at certain locations in the beam. The relative elasticity and position of each laminae appeared to dictate where concentrations were the highest; specific interelationships, however, were difficult to identify.

Most of the mappings indicated levels of strain in excess of values calculated theoretically, particularly at the beam's extreme fibers. Perhaps this reflects the use of limiting assumptions such as a perfectly rigid glueline, homogeneous elastic properties, and that size (depth) effects can be neglected. Such deficiencies in theoretical approaches would result in overly high calculations of stiffness which, in turn, would yield lower estimates of strain magnitudes at given loads.

A final characteristic feature of the experimentally obtained mappings was that the position of the neutral axis was consistently located above the predicted position. This may imply that the elasticities of the laminae are higher when stressed in compression than in tension.

5.4 The behavior of beams with a knot defect included

This aspect of the research dealt with the impact of knot position in the beam cross-section on strain distributions. Unfortunately, the dark color of the knots prevented measurement of strains within the knotwood itself; only mappings within the knot's vicinity were obtained.

Figures 5.9 and 5.10 show scatter plots of strain with the knot positioned in the extreme lamination. This beam was deflected with the defective lamination in the compression zone (Figure 5.9) and then with it in the tension zone (Figure 5.10). In the vertical cross-sections which included the knot, the two mappings were quite similar, and appeared to behave as might be expected from a beam three laminations deep. Theoretical calculations make this assumption. Strain values immediately adjacent to the knot exhibited dramatic reductions, diminishing in magnitude towards the extreme fibers - both when in the compression and tension zones. This reflects the discontinuity of longitudinal fibers caused by the encased knot. This observation, coupled with a comparison with the drawn theoretical distribution, leads one to believe that the influence of knots extends well beyond its physical margins.

A higher level of strain was observed in the extreme fibers near the knot in Figure 5.9 (subjected to compressive stresses) compared to that in Figure 5.10. This could imply that some longitudinal stresses (and strains) are transfered through the knot in this configuration. The ability to transfer stresses is important for more efficient stress distribution within the cross-section at a given load level, and was evidenced by a notable improvement in gross beam stiffness.

Figures 5.11 and 5.12 display plots for a beam with the knot located within an interior lamination. In both instances, it was apparent that strains were more highly concentrated in the extreme laminae adjacent to the knot. The strain mappings in the neighboring region exhibited little interactive response to the presence of the knot. This differs from the behavior displayed in Figures 5.9 and 5.10 where the knot lay amongst the extreme fibers. This may be partly due to the lower magnitudes of strain within the interior locations of the beam cross-section.

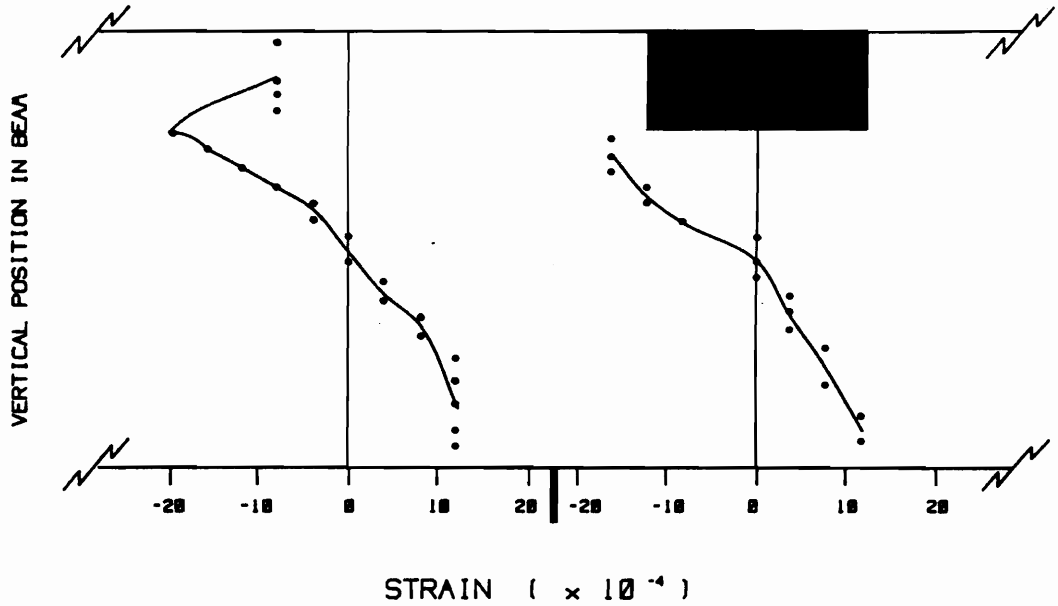

Figure 5.9 Mappings of strain in two vertical sections within a Western White Pine beam containing a knot defect in the upper extreme lamination. Measured at a 0.200" midspan deflection. Dashed line indicates theoretical distribution. (MOE = 1.24 x 10^6 psi)

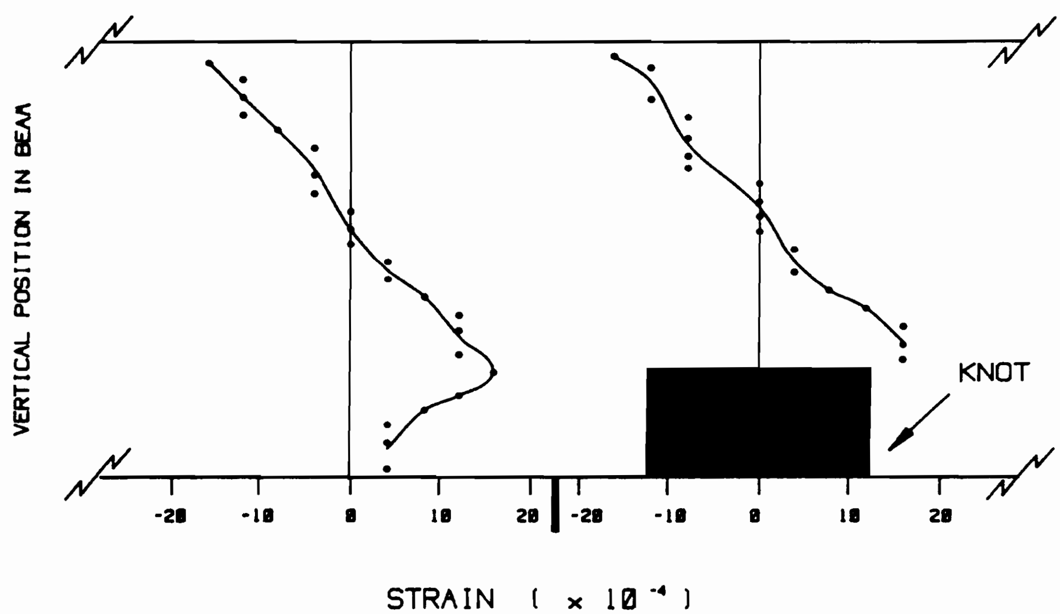

Figure 5.10 Mappings of strain in two vertical sections within a Western White Pine beam containing a knot defect in the **lower** extreme lamination. Measured at a 0.200" midspan deflection. Dashed line indicates theoretical distribution. (MOE = 1.14 x 10^6 psi)

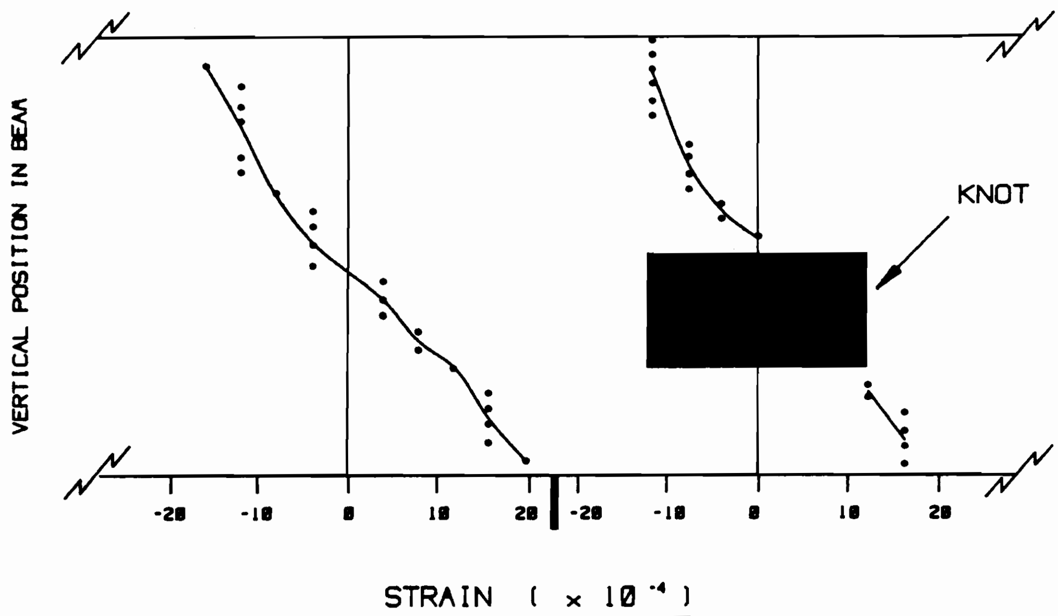

Figure 5.11 Mappings of strain in two vertical sections within a Western White Pine beam containing a knot defect in the lower interior lamination. Measured at a 0.200" midspan deflection. Dashed line indicates theoretical distribution. (MOE = 1.75 x 10^6 psi)

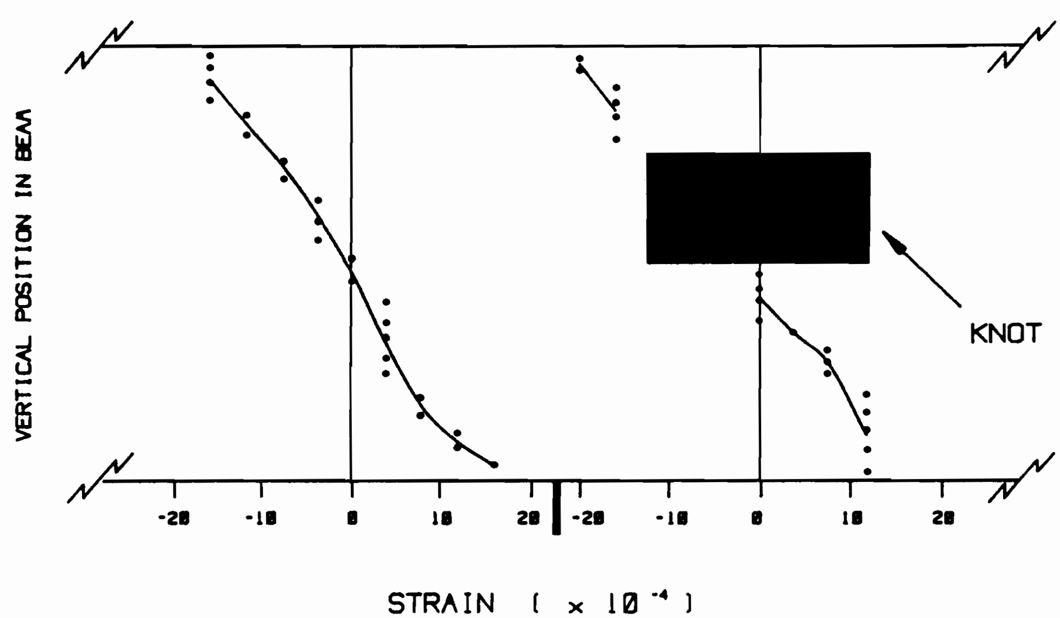

Figure 5.12 Mappings of strain in two vertical sections within a Western White Pine beam containing a knot defect in the upper interior lamination. Measured at a 0.200" midspan location. Dashed line indicates theoretical distribution. (MOE = 1.72 x 10^6 psi)

CHAPTER 6

CONCLUSIONS AND FUTURE WORK USING THE DEVELOPED TECHNIQUE

Conclusions will first be drawn concerning the experimental method. This will be followed by a brief discussion of the results derived from the technique and future applications.

The experimental technique:

An effort was made to overcome anisotropic variability in wood by reducing beam width and examining the behavior of radial/longitudinal surfaces. In this way, surface strains could be correlated to observable material structure more directly. This assertion was shown to be reasonably valid (see Appendix B), provided careful measures were taken in preparing the specimen. Higher strain resolutions and/or further reducing the width of the beam would probably improve approximations.

The optical scanning system that was developed for measuring localized surface displacements clearly lacked the resolution to enable measurement of <u>discrete</u> strains. The large deformations detected in the bending members at a 0.200" midspan deflection were, however, generally of such large magnitude that the truncated data did provide meaningful information. It is likely that more precise strain mappings could be obtained by increasing both camera and capture board resolutions.

To perhaps a lesser extent, the type and intensity of surface lighting effected strain measuring capabilities. It was noted that minute lighting changes effect definition of the dots on the wood background in the preprocessed image. Developing a more uniform means of illumination could only enhance the precision of the technique. A new sorting algorithm could easily be incorporated into the software which could detect changes in dot definition (due to lighting changes) by establishing a blob list size range.

The present scanning system was designed to measure horizontal (axial) deformations. Although somewhat limited in measuring capabilities, it served the purposes of this investigation. A notable advantage of the system is the versatility it provides for measuring strains over a broad range of dimensional levels, from microscopic to macroscopic.

Mappings of horizontal strain clearly are not adequate to <u>completely</u> describe flexural behavior, although they are generally of greatest importance. Reactions within the bending member induce a continuum of deformations within the vertical plane. To describe strains (or stresses) in two dimensions within any region of interest, the existing software would need to be modified to measure the relative displacements of four dots arranged in a rectangular configuration. Modifications of this type could easily be accomplished and would provide experimental data directly comparable with finite element models.

A final comment on the scanning system concerns the mechanism which permitted tha camera to automatically follow the beam as it deflected. The physical movement of the balance arm device during a test caused a small amount of camera rotation to occur which, in turn, altered the viewing angle slightly. Because of this, the full camera field of view could not be utilized. An improved method would involve mounting the camera on a vertical slide resting on the beam itself providing direct tracking. The light source should also be attached to this mechanism to minimize shadowing effects caused by unsequenced movements between the lighting and target surface.

Results derived from the technique:

The non-linearity of the strain distributions within the beam cross-sections may imply that interactions occuring between laminae in these composite beams creates concentrations of stress (and associated strain). This could be expected in the vicinity of knots, but is less obvious for defect-free beams consisting of laminations of mixed stiffness. Nonlinear mappings may also have been accentuated by the averaging method used to fit curves to the scatter plots of strain values with finite resolution.

Secondly, changes in the geometry of the assymetrical beams led to changes in the distributions of absolute strain (not mirror images of one another). This did not, however, seriously influence overall beam stiffness values, but does suggest possible differences in material behavior depending upon the mode of stresses present (compression or tension). The most significant consequence that such inconsistent behavior may have is in affecting ultimate load carrying capacity of the member, since progressive material deformations often culminate in the initiation of failure mechanisms (crack initiation and propagation). Therefore, distributions such as these should perhaps be considered more seriously than stiffness criteria in making an estimation of the member's ultimate bending strength.

Future work using the technique to study wood-based materials:

The feasability of using the developed technique for establishing quantitative relationships between the structure of wood-based materials and mechanical behavior under load has been demonstrated. The usefulness of the method extends to a broad range of applications in studying the mechanics of both wood and non-wood materials. The technique could aid in the development of new composite materials, or evaluating existing ones, by providing information critical to efficient design. Solid wood mechanics research would also benefit from this type of experimentally-derived data. In the area of finite element computer modelling, experimental data could be obtained on specimens comparable to those being modeled mathematically. This would enable the quality and susequent usefulness of such models to be evaluated. In addition, the mechanics of elastic and viscoelastic material deformations in highly strained regions prior to catastrophic failure would be useful for discerning true mechanisms of failure in the field of fracture mechanics.

BIBLIOGRAPHY

Al-Dabbagh, A., J.R. Goodman, and J. Bodig. 1972. Finite element method analysis for wood mechanics. Journal of Struct. Div. ASCE (ST3): 569-586.

Aplin, E.N. and F.J. Keenan. 1977. Limit states design in wood: a Canadian perspective. Forest Products Journal 27 (7): 14-18.

American Institute of Timber Construction. 1983. American national standard for wood products - structural glued laminated timber. Designation ANST/AITC A190.1.

American Society for Testing and Materials. 1986a. Establishing clear wood strength values. ASTM Designation D2555-78.

American Society for Testing and Materials. 1986b. Establishing structural grades and related allowable properties for visually graded lumber. ASTM Designation D245-74.

American Society for Testing and Materials. 1986c. Evaluating allowable properties for grades of structural lumber. ASTM Designation D-2915-74.

American Society for Testing and Materials. 1986d. Standard method for establishing stresses for structural glued-laminated timber (glulam) manufactured from visually graded lumber. ASTM Designation D3737-81.

American Society for Testing and Materials. 1986e. Standard specification for adhesives for structural laminated wood products for use under exterior (wet use) exposure conditions. ASTM Designation D2559-82.

American Society for Testing and Materials. 1986f. Standard methods of static tests of timbers in structural sizes. ASTM Designation D198-76.

American Society for Testing and Materials. 1986g. Standard methods of testing small clear specimens of timber. ASTM Designation D143-83.

Asano, I. and K. Tsuzuki. 1960. Studies of strain measurements in wood by electrical resistance wire strain guage. Journal of the Japan Wood Research Society. 6 (4): 140-144.

Barrett, J.D., and R.O. Foschi. 1977. Mode II Stress-intensity factors for cracked wood beams. Engineering Fracture Mechanics. Vol 9: 371-378.

Barrett, J.D., and R.O. Foschi. 1978. On the application of brittle fracture theory, fracture mechanics, and creep-rupture models for the prediction of the reliability of wood structural elements. In: Report of a Workshop on General Constitutive Relations for Wood and Wood-Based Materials, pp. 80-154, Dept. of Mech. Engng., Syracuse University, Syracuse, NY.

Bodig, J. and J.R. Goodman. 1973. Prediction of elastic parameters for wood. Wood Science. 5 (4): 249-264.

Bodig, Jozef and Benjamin Jayne. 1982. Mechanics of Wood and Wood Composites, Van Nostrand Reinhold Company, Inc., New York, NY. 712 pp.

Bohannan, Billy. 1966a. Flexural behavior of large glued-laminated beams. US Forest Service Research Paper FPL 72, US Dept. of Agriculture, Madison, Wisconsin. 16pp.

Bohannan, B. 1966b. Effect of size on bending strength of wood members. USDA Forest Service Research Paper. FPL 56. 19 pp.

Budynas, Richard G. 1977. Advanced Strength and Applied Stress Analysis. McGraw-Hill Book Company, New York, NY. 508pp.

Chajes, Alexander. 1974. Principles of Structural Stability Theory. Prentice-Hall, Inc., Englewood Cliffs, New Jersey. 336 pp.

Chu, T.C., W.F. Ranson, M.A. Sutton, and W.H. Peters. 1985. Applications of digital-image correlations techniques to experimental mechanics. Experimental Mechanics, September, 232-241.

Cook R.D. 1981. Concepts and Applications of Finite Element Analysis, 2nd Edition. John Wiley and Sons. New York. 537pp.

Cramer, S.M. 1984. Failure modeling of wood structural members. Ph.D. Dissertation, Department of Civil Engineering, Colorado State University, Fort Collins, Colorado.

Cunningham, J.H. and J.M. Yavorski. 1965. Strain distribution in Maple glue block shear specimen as indicated by a brittle lacquer. Forest Products Journal 5 (1): 80-86.

Ellingwood, B. 1981. Reliability of wood structural elements. Journal of the Structural Division, ASCE. 107(1): 73-87.

Etherington, M.D., R.J. Pick, and D.J. Burns. 1972. Finite element analysis of laminated wood structures. University of Waterloo.

Forrer, Johannes. 1987. Image pre-processing algorithms for isolation of defects in Douglas-fir veneer. Master of Science Thesis, Department of Forest Products, Oregon State University.

Foschi, R.O., and J.D. Barrett. 1980. Glue-laminated beam strength: A model. Journal of the Structural Division, ASCE. 106(8): 1735-1754.

Fox, S.P. 1978. Bending strength of a proposed Douglas-Fir 20f glulam stress grade: information report VP-X-175. Western Forest Products Laboratory, Canadian Forest Service, Vancouver, B.C., Canada. 12pp.

Freas, A.D. 1962. Factors affecting strength and design principles of glued laminated construction. USDA Forest Products Laboratory. Research Report 2016.

Freas, A.D., and M.L. Selbo. 1954. Fabrication and design of glued-laminated wood structural members. Technical Bulletin, November 1069. US Department of Agriculture, Washington D.C.

Fritz, D.W. 1967. The photoelastic coating method applied to the stress analysis of wood. Master of Science Thesis, Oregon State University.

Funck, J.W., Butler, D.A., and C.C. Brunner. 1987. Evaluation of image analysis routines for defect scanning on wood surfaces. Presented at 2nd Intl. Conf. on scanning technologies in sawmilling. Oakland, California. 28pp.

Galligan, W.L. and D.W. Green. 1980. Development of standardized concepts for assignment and assessment of the mechanical properties of wood. Forest Products Journal 30 (9): 39-46.

Goodman, J.R. and M.E. Criswell. 1983. Changes in design philosophy. Proceedings from: Wall and Floor Systems Design and Performance of Light-frame Structures. Forest Products Research Society, Denver, September 22-24. Proceedings 7317, pp. 7-17.

Hatayoma, Y. 1960. Mechanical properties analysis of wood by means of brittle lacquer. Journal of the Faculty of Agriculture. Iwata University 4(4): 380-387.

Itani, R.Y. and K.F. Faherty. 1984. Structural wood research, state-of-the-art and research needs. Proceedings of Workshop held at Milwaukee, Wisconsin, ASCE, New York, NY.

Keenan, F.J. and K.A. Selby. 1973. The shear strength of Douglas-fir glued-laminated timber beams. Department of Civil Engineering, University of Toronto. Publication number 73-01.

King, E.G. 1957. Creep and other strain behavior for wood in tension parallel to the grain. Forest Products Journal 5 (1): 77-84.

Linzmayer, Owen. 1985. Digital image processors: give your computer the gift of sight. Creative Computing 11 (7). 65-67.

Liu, J.Y. 1980. Shear strength of wood beams: a Weibull analysis. Journal of the Structural Division, ASCE. 106(10): 2035-2052.

Maki, A.C. and E.W. Kuenzi. 1965. Deflection and stresses of tapered wood beams. US Forest Products Laboratory Research Paper FPL 34. Madison, Wisconsin.

Marx, Catherine M., and Russell C. Moody. 1981a. Bending strength of shallow glued-laminated beams of a uniform grade. US Forest Service Research Paper FPL 380, US Department of Agriculture, Madison, Wisconsin. 19pp.

Marx, Catherine M., and Russell C. Moody. 1981b. Strength and stiffness of small glued-laminated beams with different qualities of tension laminations. US Forest Service Research Paper FPL 381. US Department of Agriculture, Madison, Wisconsin. 48pp.

Moody, Russell C. 1977. Improved utilization of lumber in glued-laminated beams. US Forest Service Research Paper FPL 292. US Department of Agriculture, Madison, Wisconsin. 49pp.

National Forest Products Association. 1982. National Design Specification for Wood Construction (A Supplement to the 1982 Edition).

Ostman, Larry. 1985. Development of techniques to study the behavior of bolted wood joints. Master of Science Thesis, Oregon State University.

Peters, W.H. and W.F. Ranson. 1982. Digital imaging techniques in experimental stress analysis. Optical Engineering 21(3): 427-431.

Phillips G.E., J. Bodig and J.R. Goodman. 1981. Flow grain analogy. Wood Science 14(2): 55-64.

Price E.W. 1967. Stress distribution in the vicinity of knot-holes in construction lumber under bending forces. Master of Science Thesis. College of Forestry, University of Washington.

Pugel, A.D. 1986. Fracture criteria for the tensile strength of wood. Ph.D. Dissertation, Department of Forest and Wood Sciences, Colorado State University.

Schniewind, A.P. 1963. Mechanism of check formation. Forest Products Journal 13(11): 475-480.

Schniewind, A.P., and R.A. Pozniak. 1971. On the fracture toughness of Douglas-fir wood. Engng. Fracture Mech. 2(3): 223-233.

Silverman, M. 1980. Flexure of laminated beams. Journal of the Structural Division, ASCE. 106(3): 711-724.

Stieda, C.K. 1965. Photo stress analysis of timber structures. In: Proceedings of Second Symposium on the Non-destructive Testing of wood. Spokane, Washington. 347-370.

Stieda, C.K. 1964. Stress concentration in notched timber beams. Transactions of the Engineering Institute of Canada (10) A5-AN.

Suddarth, S.K., and W.L. Galligan. 1978. Differential reliability: probabilistic engineering applied to wood members in bending / tension. US Forest Service Research Paper FPL 302. US Department of Agriculture, Madison, Wisconsin.

Swift, G.W., and R.A. Heller. 1974. Layered beam analysis. Journal of the Structural Division, ASCE. 100(2): 267-282.

Takahashi, A. and K. Nakato. 1964a. Strain determination of wood by using photoelastic coating technique I, II on the photoelastic characters of the modified epoxy resin. Journal of the Japan Wood Research Society 10(2): 49-61.

Takahashi, A. and K. Nakato. 1962b. Strain determination of wood by using photoelastic coating technique III on the relation between elastic modulus and the strain distribution of photoelastic coating. Journal of the Japan Wood Research Society 10(5): 176-181.

Takahashi, A. 1965. Strain determination on wood by using photoelastic coating technique IV: The strain distribution of the cross-section (log) under diametrical compression. Journal of the Japan Wood Research Society 11(1): 7-13.

Takahashi, A. 1966a. Strain determination of wood by using photoelastic coating technique VI: On the strain distribution of board with with a loose knot subjected to tensile load. Journal of the Japan Wood Research Society 12(2): 63-66.

Takahashi, A. 1966b. Strain determination of wood by using photoelastic coating technique VII: Effect of grain angle (longitudinal direction) to tensile strength and to strain distribution on wood in member with a hole. Journal of the Japan Wood Research Society 12(4): 160-165.

Tang, R.C. 1984. Stress concentration around knots in laminated beams. Wood and Fiber Science 16(1): 57-71.

USDA Forest Products Laboratory. 1987. Wood Handbook: Wood as an Engineering Material. USDA Agriculture Handbook Number 72. 466pp.

Wangaard, F.F. 1950. The Mechanical Properties of Wood. John Wiley and Sons, Inc. New York, NY.

Weathers, J.M., W.A. Foster, W.F. Swinson, and J.L. Turner. 1985. Integration of laser-speckle and finite-element techniques of stress analysis. Experimental Mechanics 25(3): 60-65.

Weibull, W. 1939. A statistical theory of the strength of materials. Proc. Roy. Swed. Inst. Engng. Res. No. 151, Stockholm.

Western Wood Products Association. 1980. Machine Stress-Rated Western Lumber: Procedures for Qualifications and Quality Control. WWPA, Portland, Oregon. 7pp.

Youngquist, W.G. 1957. Performance of bonded wire strain guages on wood. US Forest Products Laboratory Report Number 2087. US Department of Agriculture, Madison, Wisconsin.

Zakic, B.D. 1983. Shearing stress in plastic bending of wood beams. Journal of the Structural Division, ASCE. 109(4): 1042-1060.

APPENDICES

APPENDIX A

OPTICAL SCANNING SOFTWARE

Computer program written in "C" for optical scanning image acquisition and subsequent strain analysis. Function routines called by the program were previously written.

```
/*soh-----------------------------------------------------------------------
*
* hump.h:
*
**eoh----------------------------------------------------------------------

#define MAXITERATIONS 10  /* maximum number of times connectivity is run at
                    each load level to obtain averages of COLMEA and
                    ROWMEA for each dot. This was necessary due to
                    the amount of variation between two
                    consecutive run of connectivity */
#define MAXBLOBS 30    /* maximum number of blobs in an image */
#define ABSMAXTEXT 200 /* maximum length of input line */
#define TRUE 1
#define FALSE 0

typedef struct (
     double col, row;
) coords;

int thr;        /* threshold */
int num_of_iterations; /* number of times connectivity is run at each
                 load level */
int num_of_blobs;    /* number of blobs in current field */
int num_of_dots;     /* number of dots in current field */
int num_of_pairs;    /* number of dot pairs in current field */
int num_of_scans;    /* number of times connectivity will be performed
                      in the current, field. */
int ref_pair;      /* index of the reference pair */
int start, finish;
int sec_of_wait;    /* number of seconds to wait between scans */
int color_camera;   /* Boolean, TRUE if color camera is use */
char reference;     /* position of the reference dots within the
                      current field: T (top) or B (bottom). */
double ref_distance[10]; /* measured distance of first scan, without loads
double strain [10] [51]; /* strain [dot_pair] [load or scan */

/* functions */

/* hump2 */
int get_thr (void);
void bubblesort (coords [], int);
FILE *get_out_file (char[]);
void print_output (FILE *, int, int);

/* hump */
void get_input (void);
int process (void);
void calculate (FILE *, int, int );
```

```
            if ((int) a[j].row < (int) a[j+1].row) {
                 t.row = a[j].row;
                 t.col = a[j].col;
                 a[j].row = a[j+1].row;
                 a[j].col = a[j+1].col;
                 a[j+1].row = t.row;
                 a[j+1].col = t.col;
                 sorted = 0;
            }
       }
       i++;
}
}
/*soh-------------------------------------------------------------------
*  get_out_file: It allows the user to enter the name of an output file
*
* Synopsis:  FILE *get_out_file()
*
* Returned value: file handle of output file.
*
**eoh-------------------------------------------------------------------

FILE *get_out_file (textline)
char textline[];

{
FILE *fp;
char c;

/* Open file with read/write option to determine if it already exists */
fp = fopen(textline, "r");

if (fp != NULL) {   /* File pre-exists */
    fclose (fp);
    printf("\n\n\nFile %s already exists.", textline);
    printf("\nWould you like to append data to the file (Y or N)?  ");
    scanf("%1s", &c);
    if (toupper(c) == 'N')
     /* User requests file to be overwritten */
     fp = fopen(textline, "w");
    else
     /* User would like to append data to pre-existing file */
     fp = fopen(textline, "a");
}
else {
     /* File does not exist; open file for writing */
     fclose (fp);
     fp = fopen(textline, "w");
}

return fp;
}
```

```
{
char c;
int satisfied;


/* repeat loop until user is satisfied with image */
satisfied = 0;
do {
    printf("\n\nEnter threshold value:\n");
    scanf("%d", &thr);

    /* disp image, gray it, threshold it at present threshold level */
    grab_image();
    SetDispMode();
    if (color_camera) gray(0);
    thresh(0,thr);

    printf("Is this threshold value satisfactory ? (Y/N)\n");
    c = getch();
    c = toupper(c);
    if (c == 'Y') satisfied = 1;

    SetLiveMode();

} while (!satisfied);

return thr;
}


/*soh----------------------------------------------------------------------
* bubblesort:  It performs a sort in descending order of array a[], by the
*           a[].row field.
*
* Synopsis:  void bubblesort (a, n)
*         coords  a[]:  array to be sorted.
*         int n:       index of the last element of a[].
**eoh---------------------------------------------------------------------

void bubblesort (a, n)
coords a[];
int n;


{
int i;        /* no. of passes through the array */
int j;        /* index for unsorted part fo the array */
coords t;   /* variable used for element exchange */
int sorted; /* if true after current pass, then array is sorted */

i = 0;
sorted = 0;
while ((i < n) && (!sorted))  {
     sorted = 1;
     for (j = 0; j < n-i; j++) {
```

```c
/*soh----------------------------------------------------------------------------
*
* hump2.c:
*
**eoh----------------------------------------------------------------------------

#define LINT_ARGS 1  /* turn on parameter checking */
#include "v_strucs.h"
#include "v_funct.h"
#include "io.h"
#include "ctype.h"
#include "conio.h"
#include "stdlib.h"
#include "hump.h"

/*soh----------------------------------------------------------------------------
 *
 * print_output: It outputs strain values for current field of vue.
 *
 *    Synopsis:    void print_output (fp, last_scan, field)
 *            FILE *fp;
 *            int last_scan, field;
 *
**eoh----------------------------------------------------------------------------

void print_output (fp, last_scan, field)
FILE *fp;
int last_scan, field;

{
int pair, scan;

for (pair = start; pair < finish; pair++) {
   fprintf (fp, "%d %d  ", field, pair);
   for (scan = 1; scan < last_scan; scan++)  {
      fprintf (fp, "%10.4f", strain[pair][scan]);
   }
   fprintf (fp, "\n");
}

}

/*soh----------------------------------------------------------------------------
 *
 * get_thr:     This function allows the user to select an approprite
 *         threshold for the current image he is working with.
 *
 *    Synopsis:    int get_thr()
 *
 *    Value returned: threshold value selected by user.
 *
**eoh----------------------------------------------------------------------------

int get_thr()
```

```
        calculate (fp2, scan, field);

        /* wait "sec_of_wait" seconds */
        time (&current_time);
        target_time = current_time + (long) sec_of_wait;
        while (current_time < target_time) {
           time (&current_time);
        }
        if (kbhit())
           scan_again = FALSE;

        scan++;
    }

    print_output (fp, scan, field);

    printf ("\n Do you want to process another field ? (Y/N):  ");
    scanf ("%1s", &answer);
    if (toupper(answer) == 'N')
        field_again = FALSE;
    else
        field++;

} while (field_again);

sys_end ();   /* closes all files and reset targa hardware */

exit (0);

}
```

```
      strain[pair][scan] = ((distance[pair] / cf) - ref_distance[pair]) /
                     ref_distance[pair];
   }
}


}

/*-----------------------------------------------------------------------------*/
main ()

{
char answer;
int error, length;
int bl;
int scan, field;
int scan_again, field_again;
long target_time, current_time;
char textline[ABSMAXTEXT];
FILE *fp, *fp2;

printf ("\n\n Are you using a color camera ? (Y/N):  ");
scanf ("%1s", &answer);
if (toupper(answer) == 'Y')
     color_camera = TRUE;
else
     color_camera = FALSE;

/* get file name */
printf("\n\n\nEnter ouptput file name?  ");
scanf("%s",textline);
fp = get_out_file(textline);

/* create name of 2nd output file */
length = strlen(textline) - 1;
if (textline[length] == '2')
     textline[length] = '1';
else
     textline[length] = '2';
fp2 = get_out_file(textline);

sys_init();

field = 1;
field_again = TRUE;

do {
    scan = 0;
    scan_again = TRUE;
    get_input();

    while  ((scan < num_of_scans) && (scan_again)) {

        /* perform connectivity and calculate strain values */
```

```
            }
            else  {
                 errmsg (-12);
                 exit (1);
            }
         }
         idxblob++;
       }

       if (dot != num_of_dots) {
         errmsg (-12);
         exit (-12);
       }

       /* Release current blob list */
       Release_BL(bl);

       iteration++;
  }

  /* take the average of the ROWMEAN and COLMEAN values */
  for (dot = 0; dot < num_of_dots; dot++) {
       storage[dot].col = storage[dot].col / num_of_iterations;
       storage[dot].row = storage[dot].row / num_of_iterations;
  }

  /* sort the storage values in descending order of row */
  bubblesort (storage, num_of_dots - 1);

  /* calculate strains, and output to file */
  dot = 0;
  if (scan == 0) {  /* first scan of this field, no load */
     for (pair = 0; pair < num_of_pairs; pair++) {
        ref_distance[pair] = sqrt (pow(storage[dot].col - storage[dot+1].col, y)
             + pow (const * (storage[dot].row - storage[dot+1].row), y));
        dot += 2;
     }
     /* store distance of the reference pair in output file */
     fprintf (fp2, "%i %i %10.4f\n", field, scan, ref_distance[ref_pair]);
  }
  else {    /* loaded scan */
     for (pair = 0; pair < num_of_pairs; pair++) {
        distance[pair] = sqrt (pow(storage[dot].col - storage[dot+1].col, y)
             + pow (const * (storage[dot].row - storage[dot+1].row), y));
        dot += 2;
     }
     /* store distance of the reference pair in output file */
     fprintf (fp2, "%i %i %10.4f\n", field, scan, distance[ref_pair]);

     /* calculate correction factor */
     cf = distance[ref_pair] / ref_distance[ref_pair];

     /* strains */
     for (pair = start; pair < finish; pair++) {
```

```
        exit(1);
    }

    SetLiveMode();

    return (bl);

}

/*sch-------------------------------------------------------------------
*
* calculate
*
**ech------------------------------------------------------------------ */

void calculate (fp2, scan, field)
FILE *fp2;
int scan, field;

{
int bl, dot, idxblob, pair, iteration;
BLOB *bptr;
BCB *blist_hdl;
coords storage[MAXBLOBS];   /* storage for average COLMEAN and ROWMEAN */
double distance[10];           /* measured distances of scans > 0 */
double cf;                  /* correction factor */
double y = 2.0;             /* used in pow function to obtain the 2nd power */
double const = 1.09;           /* to compensate for the x/y ratio of the screen */

/* set elemetns of storage[] to 0.0  */
for (dot = 0; dot < MAXBLOBS; dot++) {
     storage[dot].col = 0.0;
     storage[dot].row = 0.0;
}

iteration = 0;
while (iteration < num_of_iterations) {
     /* perform connectivity analysis */
     printf ("\n Performing iteration number %d of scan number %d",
           iteration + 1,  scan + 1);
     bl = process();

     /* set index to first blob */
     idxblob = 0;
     blist_hdl = blist[bl];

     dot = 0;  /* index for temporary storage of dot info */
     while (idxblob < num_of_blobs) {
       bptr = blist_hdl->BLIST[idxblob];
       if (bptr->COLOR == 0) {
          if (dot < MAXBLOBS) {
              storage[dot].col += bptr->COLMEAN;
              storage[dot].row += bptr->ROWMEAN;
              dot++;
```

```
printf ("\n\n Do you want to reset the window size ? (Y/N):  ");
scanf ("%1s", &answer);
answer = toupper (answer);
if (answer == 'Y') {
     curr_window.LEFT_COL = 256;
     curr_window.BOTTOM_ROW = 200;
     curr_window.RIGHT_COL = 256;
     curr_window.TOP_ROW = 200;
     SetDispMode();
     printf ("\n\n Press any key to set new window bottom-left corner.");
     cursor (&curr_window.LEFT_COL, &curr_window.BOTTOM_ROW);
     printf ("\n\n Press any key to set new window top_right corner.");
     cursor (&curr_window.RIGHT_COL, &curr_window.TOP_ROW);
     error = SetBothWindows (0, &curr_window);
     if (error < 0) {
          errmsg (error);
          exit (error);
     }
     SetLiveMode();
}
else
     SetFullWindows(0);

}

/*soh--------------------------------------------------------------------
 *
 * process:
 *
**eoh------------------------------------------------------------------ */

int process()

{
int bl;
int error;

    grab_image();
    SetDispMode();
    if (color_camera) gray(0);
    thresh(0,thr);

    /* Create blob list and perform connectivity analysis for window */
    bl = Create_BL(num_of_blobs, 1, 0, 0, 0);
    if (bl < 0) {
     errmsg(bl);
     exit(1);
    }

    /* perform connectivity analysis for blob list */
    error = Connectivity(0, bl);
    if (error < 0) {
       errmsg(error);
```

```
");
   scanf ("%d", &num_of_dots);
   if (num_of_dots <= 20) {
      num_of_blobs = num_of_dots + 10;
      num_of_pairs = num_of_dots / 2;
      done = 1;
   }
   else  {
      printf ("\n To many dots, try again.");
   }
} while (!done);


printf ("\n Enter position of the reference dots (T/B):  ");
scanf ("%1s", &reference);
reference = toupper (reference);
if (reference == 'T') {
   ref_pair = 0;
   start = 1;
   finish = num_of_pairs;
}
else  {
   ref_pair = num_of_pairs - 1;
   start = 0;
   finish = num_of_pairs - 1;
}

done = 0;
do {
   printf ("\n Enter # of times each scan should be repeated");
   printf ("\n to obtain average distances (1-10): ");
   scanf ("%d", &num_of_iterations);
   if (num_of_iterations < 1)
      printf ("\n Wrong !!!!!!!!!!!!, try again.");
   else if (num_of_iterations > MAXITERATIONS)
      printf ("\n To many iterations, try again.");
   else
      done = 1;
} while (!done);

printf("\n\n Enter # of seconds to wait between scans:  ");
scanf ("%d", &sec_of_wait);

done = 0;
do {
   printf ("\n\n Enter # of scans to perform on the current field ( <= 50):  ");
   scanf ("%d", &num_of_scans);
   if (num_of_scans <= 50) {
      done = 1;
   }
   else {
      printf ("\n Too many scans, try again.");
   }
} while (!done);
```

```
/*soh------------------------------------------------------------------
*
* hump.c:   This standalone program allows the user to run connectivity
*           on an image of a board displaying a series of dots.  These
*           dots are grouped into pairs, each pair on a separate row of
*           the image. Connectivity is run a  variable number of times on
*           the same field of view as the load on the beam is increased.
*           In turn, for each load level connectivity is repeated a variable
*           number of times, to obtain averages of the ROWMEAN and COLMEAN for
*           each dot. This was necessary to compensate for the amount of
*           variation observed in ROWMEAN and COLMEAN values between
*           consecutive runs of connectivity.
*           The x (COLMEAN) and y (ROWMEAN) positions of each dot centroid
*           are used  to calculate the distance between them.
*           Strain is calculated as a function of the  change in
*           distance between dots.
*
*     (c) 1987 by the Forest Products Department of Oregon State University
*
*       Author: Alberto G. Maristany, March 1987.
*
**eoh----------------------------------------------------------------- */

#define LINT_ARGS 1  /* turn on parameter checking */
#include <ctype.h>
#include <conio.h>
#include <io.h>
#include <math.h>
#include <stdlib.h>
#include <string.h>
#include <time.h>
#include "v_strucs.h"
#include "v_funct.h"
#include "main_shl.h"
#include "hump.h"

/*soh------------------------------------------------------------------
* GET_INPUT:
*
**eoh----------------------------------------------------------------- */

void  get_input()

{
struct WINDOW curr_window;
char answer;
int error;
int done;

thr = get_thr();

done = 0;
do {
   printf ("\n Enter # of dots in this field, including reference dots (2-20):
```

APPENDIX B

STRAIN UNIFORMITY ACROSS THE WIDTH OF A TYPICAL THIN BENDING MEMBER

In the present research, gradients of strain perpendicular to the beam face were assumed to be negligible. A brief verification study was conducted at two cross-section locations within a beam containing a knot defect in the top lamination. The figure below shows plots of surface strain obtained from both faces of the beam.

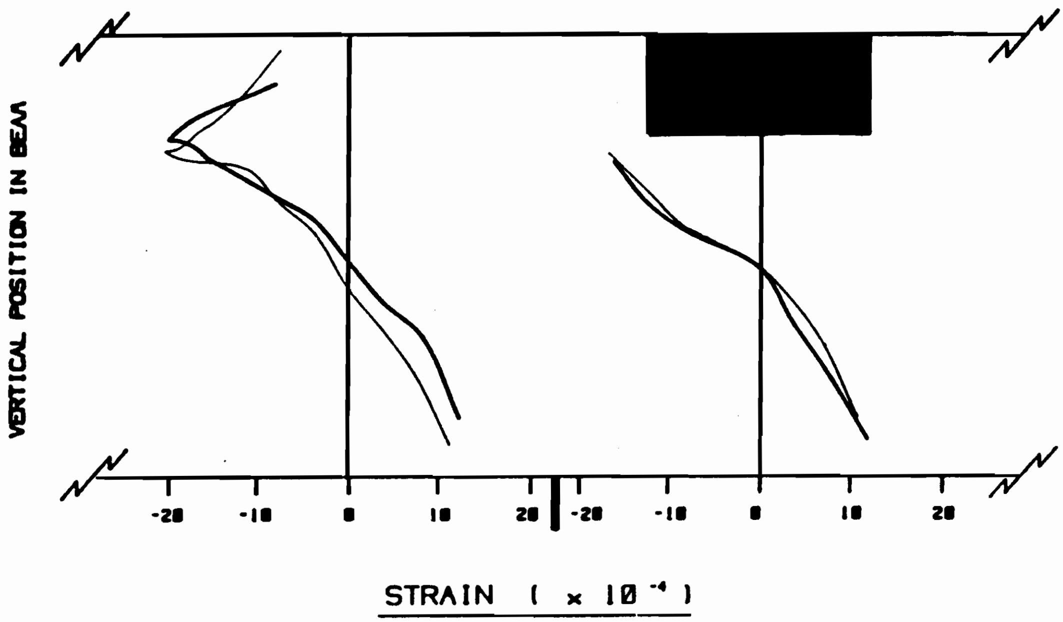

Superimposed strain mappings in two vertical sections within a Western White Pine beam containing a knot defect in the upper extreme lamination. Thin and thick lines represent measurements taken from front and back faces of the beam respectively. Measured at a 0.200" midspan deflection.